

Higgs branch RG flows via decay and fissionAntoine Bourget,^{1,*} Marcus Sperling,^{2,†} and Zhenghao Zhong^{3,‡}¹*Université Paris-Saclay, CNRS, CEA, Institut de physique théorique, 91191, Gif-sur-Yvette, France*²*Fakultät für Physik, Universität Wien, Boltzmanngasse 5, 1090 Wien, Austria*³*Mathematical Institute, University of Oxford, Andrew Wiles Building, Woodstock Road, Oxford, OX2 6GG, United Kingdom*

(Received 22 February 2024; accepted 8 April 2024; published 21 June 2024)

Magnetic quivers have been an instrumental technique for advancing our understanding of Higgs branches of supersymmetric theories with eight supercharges. In this work, we present the “decay and fission” algorithm for unitary magnetic quivers. It enables the derivation of the complete phase (Hasse) diagram and is characterized by the following key attributes: First and foremost, the algorithm is inherently simple, just relying on convex linear algebra. Second, any magnetic quiver can only undergo decay or fission processes; these reflect the possible Higgs branch RG flows (Higgsings), and the quivers thereby generated are the magnetic quivers of the new RG fixed points. Third, the geometry of the decay or fission transition (i.e., the transverse slice) is simply read off. As a consequence, the algorithm does not rely on a complete list of minimal transitions, but rather outputs the transverse slice geometry automatically. As a proof of concept, its efficacy is showcased across various scenarios, encompassing superconformal field theories from dimensions 3 to 6, instanton moduli spaces, and little string theories.

DOI: [10.1103/PhysRevD.109.126013](https://doi.org/10.1103/PhysRevD.109.126013)**I. INTRODUCTION**

The Higgs mechanism is a well-known concept in quantum field theories (QFTs) wherein a scalar field acquires a vacuum expectation value (VEV) that subsequently breaks the gauge symmetry [1–4]. For example, the electroweak theory has a $SU(2) \times U(1)$ gauge symmetry, and when the scalar field (Higgs boson) acquires a nonzero VEV, the symmetry is broken to $U(1)$. Such a Higgsing also constitutes a phase transition in the theory. Supersymmetric QFTs with eight supercharges in space-time dimensions 3–6 generically possess a continuous space of vacua known as the Higgs branch, denoted \mathcal{H} . As the Higgs branch is parametrized by many scalar fields, the theory can be Higgsed in multiple ways. This rich structure can then be encoded in a phase diagram [5].

Phase diagrams are important as they show how various theories are related to each other through means such as mass deformations, tuning of gauge couplings, Coulomb branch deformations, etc. In this paper, we derive phase

diagrams that encode how different theories are related via the (partial) Higgs mechanism or, to be more precise, Higgsing along the Higgs branch.¹ While performing a partial Higgs mechanism might not pose significant challenges for theories with known Lagrangian descriptions, the realm of superconformal field theories (SCFTs) frequently lacks such descriptions, particularly in space-time dimensions 4–6. Thus, to investigate characteristics of SCFTs, such as their Higgs branches, new methods had to be devised. One particularly powerful technique that allows one to study the Higgs branches of gauge theories and SCFTs, regardless of their space-time dimension, and even little string theories is the “magnetic quiver” [6–36].

Consider a theory \mathcal{T} in space-time dimension $d = 3, 4, 5, 6$ with eight supercharges: the magnetic quiver is a 3D $\mathcal{N} = 4$ (generalized) quiver gauge theory whose Coulomb branch is, by construction, the same as the Higgs branch of \mathcal{T} . If the Higgs branch is a union of several hyper-Kähler cones, then there exist several magnetic quivers, one for each cone [32,37]. Therefore, studying the magnetic quiver is an indirect path of studying the Higgs branch of \mathcal{T} . We pursue this indirect route due to the array of recently developed techniques tailored for the study of the Coulomb branch of 3D $\mathcal{N} = 4$ theories, starting with [38–40]. This transforms a historically challenging subject into a realm of familiarity and ease.

¹In the literature, this has also been called “Higgs branch deformations” or “Higgs branch RG flows.”

*antoine.bourget@ipht.fr

†marcus.sperling@univie.ac.at

‡zhenghao.zhong@maths.ox.ac.uk

Published by the American Physical Society under the terms of the [Creative Commons Attribution 4.0 International license](https://creativecommons.org/licenses/by/4.0/). Further distribution of this work must maintain attribution to the author(s) and the published article’s title, journal citation, and DOI. Funded by SCOAP³.

In [5], an algorithm, which we henceforth refer to as the “quiver subtraction” algorithm, was introduced. The algorithm provides the stratification of the Higgs branch of \mathcal{T} , encoding it in a phase diagram called a (Higgs branch) “Hasse diagram.” This phase diagram encodes much of the Higgs branch, including the nature of the transverse space between Higgsed theories. However, starting from \mathcal{T} , this algorithm is unable to determine the set of possible theories \mathcal{T}_i to which \mathcal{T} can be Higgsed.

While being a powerful approach that has found widespread application [9,10,13,15,17,18,21,26–28,30,34–36,41–46], the quiver subtraction algorithm is plagued by a few shortcomings: First, the algorithm requires a list of all possible elementary slices. This list is mathematically complete for the class of nilpotent orbits closures [47–49], but more general symplectic singularities may include other minimal slices. Such a new isolated symplectic singularity has recently been described in [50]. Second, it requires the knowledge of all possible quiver realization of the elementary slices. For example, the (closure of the) minimal nilpotent orbit of E_6 has, up to now, four known magnetic quiver realizations: a unitary affine Dynkin quiver, a unitary twisted affine Dynkin quiver, an orthosymplectic quiver [10,12], and a folded orthosymplectic quiver [51]. Third, quiver subtraction is only partially understood in the case of repeated identical transitions—leading to “decorated quivers” [52], which are, for example, relevant for moduli spaces involving multiple instantons. At present, it is unclear how to define the Coulomb branch of the decorated quiver; however, the quiver subtraction algorithm supplemented by decorations passed numerous consistency checks.

This paper serves to fill this gap by expanding and further developing the decay and fission algorithm [53] for magnetic quivers, whereby the diagram is generated by recursively Higgsing, i.e., starting from the bottom leaves. In a nutshell, the main results of this paper are as follows:

- (i) The Higgs branch phase diagram is shown to coincide with the Hasse diagram of simple objects in convex linear algebra. It does not require any *a priori* knowledge of the list of possible elementary transitions.
- (ii) Elementary slices, which correspond to elementary Higgsing phase transitions, are associated with one of two fundamental processes that magnetic quivers can undergo:
 - (a) Decay, where the magnetic quiver reduces to one with smaller rank. There are infinitely many decay types, which correspond geometrically to infinitely many elementary slices.
 - (b) Fission, where the magnetic quiver splits into two parts, while preserving the total rank. There

are only two fission types and, correspondingly, two possible elementary slices.

Figure 1 displays a cartoon version of these transitions.

- (iii) The decay transitions above can be implemented practically: upon inspection of balanced subquivers and overbalanced nodes, decay transitions can be read off.

The decay and fission algorithm not only reproduces the results of the standard quiver subtraction, but also allows one to deduce the daughter theories \mathcal{T}_i and grand-daughter theories \mathcal{T}'_i , etc. obtained from partial Higgsing. Of course, the information within the magnetic quiver does not comprehensively encode all aspects of \mathcal{T} . To be more accurate, the decay and fission algorithm enables one to deduce the Higgs branches for \mathcal{T}_i , \mathcal{T}'_i , and so forth. Understanding these Higgs branches provides extensive information that almost always enables one to identify the theories after Higgsing through existing literature. If not, the absence of literature suggests a potentially new theory, where the algorithm predicts its Higgs branch structure.

The true strength of this algorithm lies in its inherent simplicity. In contrast to standard quiver subtraction, which needs to introduce additional gauge groups with successive subtractions, the decay and fission algorithm never requires new nodes and simplifies the magnetic quivers with each step. This characteristic not only streamlines the process, but also facilitates the creation of a computer algorithm. Furthermore, when addressing complicated quivers, the full phase or Hasse diagram can often be exceedingly complex, rendering it less practical for analysis. The decay and fission algorithm, serving as a partial Higgsing technique, eliminates the need to construct the entire phase diagram for valuable insights. For instance, one can halt the procedure as soon as one arrives at theories that with which one is already familiar.

A. Comparison to other methods of Higgsing

For supersymmetric theories with eight supercharges, there are many different approaches to Higgsing; for instance, the Higgsing of class \mathcal{S} theories via closing of partial punctures [54]. However, the shortcomings of this and most other Higgsing algorithms include the following:

- (a) the Higgsing may not be minimal;
- (b) the exact nature (e.g., a Kleinian singularity) of the transverse space is not known; and
- (c) it does not contain some of the more unconventional Higgsings (e.g., transitions that cause the magnetic quiver to fission).

The decay and fission algorithm addresses all these shortcomings and still remains a very simple and straightforward algorithm that can be applied to any Supersymmetric theory

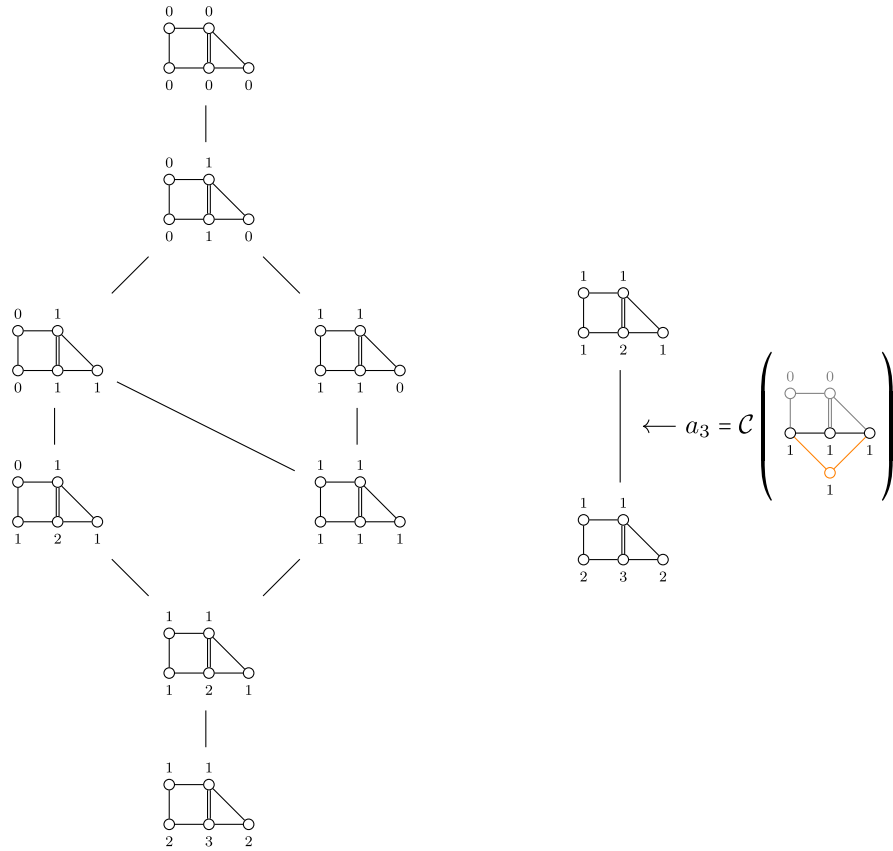


FIG. 2. Hasse diagram obtained from decays of the quiver (2.1) (left) and example of the subsequent computation of the geometry of an elementary transverse slice (right).

theory” and the other vertices are “daughter/granddaughter” theories that can be reached from the mother theory via the Higgs mechanism. We note that in some physics literature the mother theory is placed at the top instead, thus leading to an inverted picture.

II. DECAY AND FISSION

All the results of this paper rely on one simple idea, which was presented in essence in the letter [53] and in much more detail, with important additions, in this section. To help readers get familiar with this idea, we provide an intuitive description in Sec. II A. Combined with the practical realization in Sec. II C, most of the examples in Sec. III can then be worked out. Section II B gives a precise (but maybe somewhat indigested) formulation of the fission and decay algorithm. It can be skipped at first reading, but it is necessary to grasp fully certain peculiarities discussed in Sec. III. Finally, an implementation in *Mathematica* is provided in [55].

A. Intuitive statement

1. An example with decay only

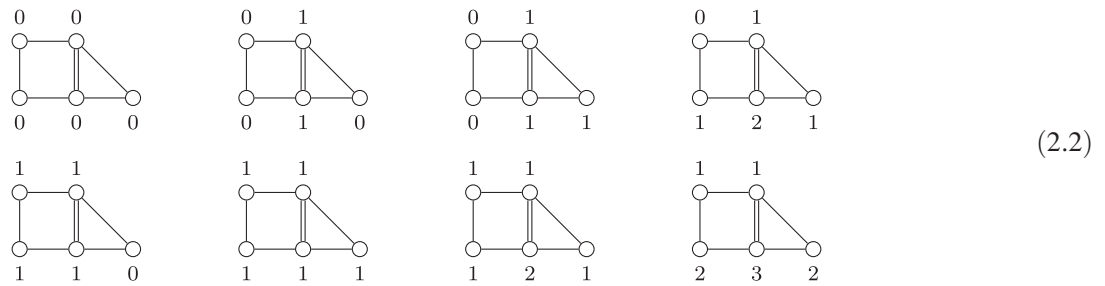
Consider a good unitary quiver \mathbf{Q} , seen as a magnetic quiver for the Higgs branch of a given theory. For instance,

$$\begin{array}{c}
 \circ \\
 | \\
 \circ \\
 | \\
 \circ
 \end{array}
 \begin{array}{c}
 \circ \\
 | \\
 \circ \\
 | \\
 \circ
 \end{array}
 \begin{array}{c}
 \circ \\
 | \\
 \circ \\
 | \\
 \circ
 \end{array}
 \begin{array}{c}
 \circ \\
 | \\
 \circ \\
 | \\
 \circ
 \end{array}
 \begin{array}{c}
 \circ \\
 | \\
 \circ \\
 | \\
 \circ
 \end{array}
 \tag{2.1}$$

We say the quiver is *good* if each node has non-negative balance.

We then compile the list of all good quivers with the same shape² and with ranks on each node smaller or equal to those in \mathbf{Q} —such quivers are said to be smaller or equal to \mathbf{Q} , and this defines a partial order \leq . In the example (2.1), we find exactly eight such quivers, namely,

²As explained in Sec. II B, one needs to remove from this list the quivers that correspond to moduli spaces of instantons.



Note that, if we add up any two nonzero quivers in this list, we end up with a quiver that is not smaller or equal to Q . This means that the quiver cannot fission (the next example contains fissions). Therefore, it can only *decay*, and the decay products are precisely the eight quivers above. The partial order between them can be summarized using a Hasse diagram, obtained by comparing in all possible ways the eight quivers in (2.2), which gives

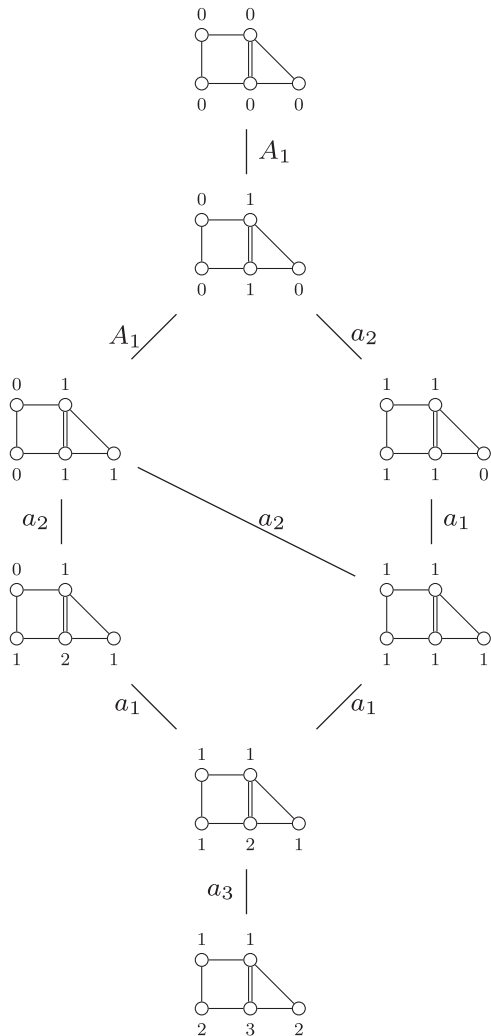


FIG. 3. Diagrams of decays from Fig. 2 with the geometry of elementary transverse slices.

25 pairs out of the $\binom{8}{2} = 28$ possible pairs of distinct quivers, and deleting a pair $Q_1 < Q_2$ if there exists Q_3 such that $Q_1 < Q_3 < Q_2$. The diagram is shown on the left of Fig. 2.

We claim this is the Coulomb branch diagram for Q in (2.1). The nature of the transverse slices can be read out from the difference of the two quivers at the ends of each edge. More precisely, align the two quivers, subtract the smaller one from the larger one, and rebalance³; then the Coulomb branch of the rebalanced quiver is the transverse slice. This is illustrated on the right of Fig. 2.

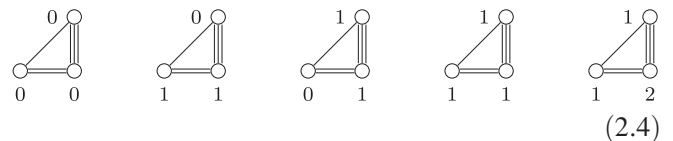
We insist on the fact that the Hasse diagram is obtained first, and the elementary transitions are computed in a second step. This is the main difference with the quiver subtraction algorithm, which is an iterative process in which elementary transitions are an input. Repeating a computation similar to the right of Fig. 2 for all elementary transitions, one obtains the final diagram of Fig. 3.

2. An example with fission

It can also happen that the sum of two or more nonzero good quivers that are $\leq Q$ is also $\leq Q$. When this is the case, the quiver (or one of its decay products) can *fission* successively into smaller parts, and each part keeps decaying and fissioning, following the same rules. For instance, consider the quiver



There are exactly five good lower quivers,



³Again, the precise way of rebalancing is given in Sec. II B. In general, it can involve a non-simply-laced edge.

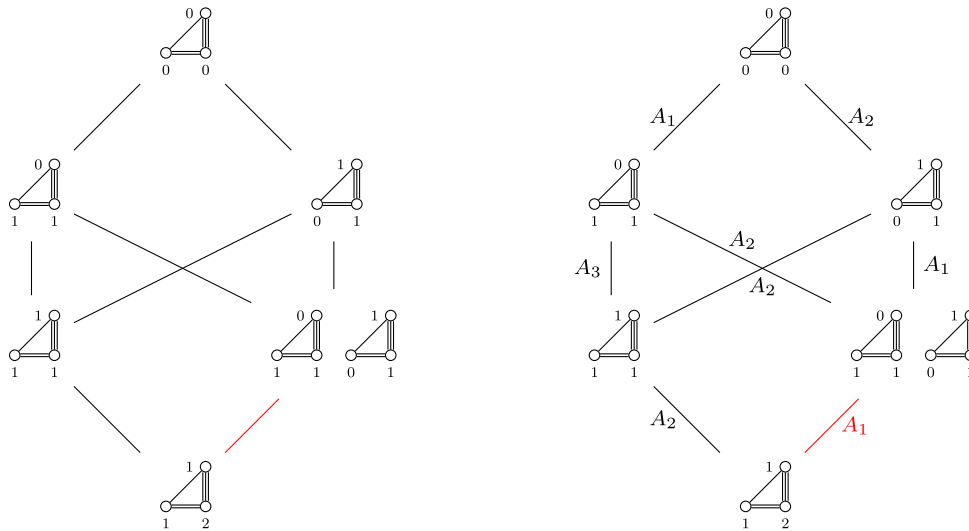


FIG. 4. Hasse diagram obtained from decays and fissions of the quiver (2.3) (left) and the same diagram after the geometry of the transverse slices has been computed (right). The red line denotes the only fission transition, all other transitions are decays.

and, among them, there is a pair of quivers whose sum gives the original quiver. This means the latter can fission,

$$\begin{array}{c} 0 \\ \circ \\ \parallel \\ \circ \\ \parallel \\ \circ \\ 1 \quad 1 \end{array} + \begin{array}{c} 1 \\ \circ \\ \parallel \\ \circ \\ \parallel \\ \circ \\ 0 \quad 1 \end{array} = \begin{array}{c} 1 \\ \circ \\ \parallel \\ \circ \\ \parallel \\ \circ \\ 1 \quad 2 \end{array} \quad (2.5)$$

The Coulomb branch Hasse diagram of (2.3) is therefore given in the left part of Fig. 4. The nature of the transverse slice corresponding to fission is obtained by comparing the greatest common divisors (gcd’s) of the ranks of the fission products [for each of the eight quivers in (2.2), this gcd is equal to 1]. When they are equal, the transverse slice has an A_1 geometry (this is the case here). When they are different, the geometry is the non-normal slice m [49,56]. In the present case, the red transition in Fig. 4 corresponds to A_1 , while all other transitions are computed using the rebalancing as in Fig. 2. We finally get the result shown in the right part of Fig. 4.

Note that prominent examples for fission arise from k -instanton moduli spaces with $k > 1$ [39], \mathcal{S} -fold theories [17], magnetic quivers of rank-2 4D SCFTs [21], 6D $\mathcal{N} = (1, 0)$ (higher-rank) E-string theories [7], etc. Even a simple class \mathcal{S} theory such as T_6 possesses this feature. Section III contains a selection of illustrative examples.

B. Formal statement

The previous subsection gave an overview of the algorithm. We now provide all the technical details, beginning with introducing the appropriate formalism.

Let \mathbf{Q} be a unitary quiver. It is convenient to encode a quiver using a matrix, which encodes the underlying

graph, and a rank vector, which specifies the ranks of the unitary groups at each node. This leads us to the following definitions.

1. Definitions

Let n be a positive integer. We define a partial order on \mathbb{Z}^n as follows. We say that $K \in \mathbb{Z}^n$ is non-negative, written $K \geq 0$, if all its entries are non-negative, i.e., if $K \in \mathbb{N}^n$. Then, given two elements $K_1, K_2 \in \mathbb{Z}^n$, we say that $K_1 \leq K_2$ if $K_2 - K_1 \geq 0$.

A quiver \mathbf{Q} with n nodes is a pair (A, K) , where A is an $n \times n$ matrix with coefficients in \mathbb{Z} and $K \in \mathbb{N}^n$ is the rank vector, such that

- (i) A has diagonal coefficients $A_{i,i} = -2 + 2g$ where $g \in \mathbb{N}$.
- (ii) The off-diagonal coefficients $A_{i,j}$ of A are non-negative integers with either $A_{i,j} = A_{j,i} = 0$ or $A_{i,j}A_{j,i} \neq 0$, and in this last case, either $A_{i,j}|A_{j,i}$ or $A_{j,i}|A_{i,j}$.
- (iii) The “balance vector” $B := AK$ has non-negative entries $B_i \geq 0$.

When $A_{i,j} = A_{j,i}$, we draw $A_{i,j}$ links between nodes i and j . When $0 < A_{i,j}|A_{j,i}$, we draw $A_{i,j}$ arrows, each of them $\frac{A_{j,i}}{A_{i,j}}$ laced, from node j to node i . The balance b of the i th node is the i th entry of the balance vector, $b = B_i$. In some drawings, when no confusion is possible, only the nodes with $K_i > 0$ are represented, with the value K_i indicated next to the node.

We say that a quiver is “reducible” if it contains a $U(1)$ node on the long side such that, when this node is deleted, the quiver breaks into several connected

components. We assume the quiver under consideration is “not reducible.”⁴

2. Leaves

Given a quiver, defined by (A, K) , let $K' \in \mathbb{Z}^n$ such that $0 \leq K' \leq K$ and $AK' \geq 0$. We define the property

$$\mathcal{P}_1(K') = [(K')^t A(K') \geq 0 \quad \text{and} \quad (K')^t (K') = 1]. \quad (2.6)$$

This property \mathcal{P}_1 simply detects the subquivers of the form $U(1)$ with one or more adjoints. We also define the property $\mathcal{P}_2(K')$ as follows. First, define for $1 \leq i \leq n$ the vector $\delta(i) \in \mathbb{N}^n$ by $\delta(i)_j = \delta_{i,j}$. Then $\mathcal{P}_2(K')$ is true if there exists a “long node” index $1 \leq i \leq n$ such that $K'_i > 0$ and, defining $K'' = K' - \delta(i)$, for all j , $(AK'')_j \times (K'')_j = 0$ (no sum on j) and $\gcd(K'') = (K'')^t A \delta(i)$. This detects the subquivers that correspond to instanton moduli spaces.⁵

Consider now the finite set

$$\mathcal{V} = \{K' | K' \in \mathbb{N}^n, K' \leq K, AK' \geq 0, \text{ not } \mathcal{P}_1(K'), \text{ not } \mathcal{P}_2(K')\}, \quad (2.7)$$

and the set

$$\mathcal{V}_0 = \{K' \in \mathcal{V} | K' \neq 0\}. \quad (2.8)$$

The elements of \mathcal{V} are the possible decay and fission products. We now just have to assemble them in all possible ways. We define $\mathcal{L}_0 = \{\emptyset\}$ and, for $m \in \mathbb{N}_{>0}$,

$$\mathcal{L}_m = \{ \{ \{ K'_1, \dots, K'_m \} \} | \forall 1 \leq j \leq m, K'_j \in \mathcal{V}_0 \text{ and } K'_1 + \dots + K'_m \leq K \}. \quad (2.9)$$

Elements of \mathcal{L}_m are the multisets⁶ of m vectors of \mathcal{V}_0 whose sum is $\leq K$ (repetitions are allowed).⁷ Finally, we write

$$\mathcal{L} = \bigcup_{m \in \mathbb{N}} \mathcal{L}_m. \quad (2.10)$$

This is the set of vertices of the Hasse diagram, which correspond to the symplectic leaves of the 3D Coulomb branch of the initial quiver (A, K) . Note that $\mathcal{L}_m = \emptyset$ for $m \gg 1$, so the above union is finite. For an element $\ell \in \mathcal{L}$, there is a unique $m \in \mathbb{N}$ such that $\ell \in \mathcal{L}_m$; we call it the “length” of ℓ , denoted $\text{length}(\ell)$. We also denote by $\Sigma \ell \in \mathbb{N}^n$ the sum of the elements of ℓ .

3. Partial order

We now have to define a partial order on \mathcal{L} . Let $\ell_1, \ell_2 \in \mathcal{L}$. We write $\ell_1 \rightsquigarrow \ell_2$ if

$$\begin{aligned} |\text{length}(\ell_1) - \text{length}(\ell_2)| &\leq 1 \\ \text{and } |\ell_1 \cap \ell_2| &= \text{length}(\ell_1) - 1 \\ \text{and } \Sigma \ell_1 &\geq \Sigma \ell_2. \end{aligned} \quad (2.11)$$

The relation \rightsquigarrow is reflexive and antisymmetric, but not transitive in general. Let us denote by \succeq its transitive closure, i.e., $\ell_1 \succeq \ell_2$ if there exists a chain $\ell_1 \rightsquigarrow \dots \rightsquigarrow \ell_2$. This is a partial order relation. We claim that (\mathcal{L}, \succeq) coincides with the partially ordered set (poset) of symplectic leaves in the 3D Coulomb branch of the quiver. This concludes our construction of the Hasse diagram.

4. Elementary transitions

The last ingredient we need is the geometry of the transverse slice between two adjacent leaves in the partial order, which is a minimal degeneration. Let $\ell_1 \succeq \ell_2$ be two adjacent leaves, i.e., such that $\ell_1 \neq \ell_2$ and there is no leaf $\ell_3 \neq \ell_1, \ell_2$ satisfying $\ell_1 \succeq \ell_3 \succeq \ell_2$. Since they are adjacent, they satisfy (2.11). There are three possibilities, depending on the value of $\text{length}(\ell_1) - \text{length}(\ell_2)$:

- (i) If $\text{length}(\ell_1) - \text{length}(\ell_2) = +1$, then $\ell_2 \subset \ell_1$. The transition corresponds to the Coulomb branch of the unique element in $\ell_1 \setminus \ell_2$; let μ be its multiplicity in the multiset ℓ_1 . This is a “terminal decay”: one quiver disappears entirely. The geometry of the transition is simply given by a union of μ copies of the Coulomb branch of the vanishing quiver.

⁴When a quiver is reducible, the corresponding theory is a product, and all its features factorize. Therefore, we focus on irreducible quivers, and it is always implied that whenever a reducible quiver is reached in the algorithm, it should be reduced and each irreducible part should be studied separately.

⁵We can unpack condition $\mathcal{P}_2(K')$ as follows. The idea is that a quiver corresponds to moduli space of instantons if there is a $U(1)$ node that is connected to a subquiver by one simply laced edge, and that subquiver is by itself fully balanced after deletion of the $U(1)$ node.

⁶A multiset can be seen as a set where elements can have multiplicities, i.e., appear more than one time or, equivalently, as a list up to permutation. We denote multisets with the symbols $\{\{\cdot\cdot\cdot\}\}$. For instance, $\{\{5, 5, 2\}\} = \{\{5, 2, 5\}\} \neq \{\{5, 2\}\}$. The multiplicity of 5 in $\{\{5, 5, 2\}\}$ is 2, and the multiplicity of 2 is 1.

⁷For our example (2.3), \mathcal{V} consists of the five vectors listed in (2.4), $\mathcal{V}_0 \simeq \mathcal{L}_1$ consists of the four vectors on the right of (2.4), and \mathcal{L}_2 has only one element, namely, the pair that corresponds to (2.5). All $\mathcal{L}_{m>2}$ are empty.

- (ii) If $\text{length}(\ell_1) - \text{length}(\ell_2) = 0$, there is a unique $K_1 \in \ell_1 \setminus \ell_2$ and a unique $K_2 \in \ell_2 \setminus \ell_1$. Let μ be the multiplicity of K_1 in the multiset ℓ_1 . The transition is a nonterminal decay from K_1 to K_2 . Let \mathbf{Q} be the quiver obtained from $K_1 - K_2$ by rebalancing using one additional $U(1)$ node with an adjoint for each connected component K_2^α of K_2 : the rebalancing is done using $\gcd(K_2^\alpha)$ -laced edges, pointing toward the new $U(1)$ node. Then the geometry of the transition is the union of μ copies of the Coulomb branch of \mathbf{Q} .⁸
- (iii) If $\text{length}(\ell_1) - \text{length}(\ell_2) = -1$, there is a unique $K_1 \in \ell_1 \setminus \ell_2$ and exactly two vectors $K_2, K_2' \in \ell_2 \setminus \ell_1$. This corresponds to fission. Let μ be the multiplicity of K_1 in the multiset ℓ_1 . If the quiver contains zero or one loop, the geometry of the transition is $\mu \cdot A_1$ if $\gcd(K_2) = \gcd(K_2')$ and $\mu \cdot m$ if $\gcd(K_2) \neq \gcd(K_2')$. For two loops or higher, a generalization is needed and is left for future work.⁹

5. Derivation

We do not have a formal proof that the algorithm presented here is correct. Rather, we have used a physical, almost experimental approach, and this should be kept in mind. We have combined insights from various perspectives in order to infer general rules that we have tested in as many cases as possible, finding in all cases perfect agreement. Specifically, the algorithm was built from

- (i) comparison with the quiver subtraction algorithm (including decorations, if needed);
- (ii) physical intuition coming from 3D mirror symmetry and brane physics, as reviewed in Sec. III A—for simple classes of quivers, this constitutes a proof of the algorithm;
- (iii) agreement with the Higgs mechanism when a weakly coupled description is available, as exemplified in Sec. II D (our results are also compatible with partial results in class \mathcal{S} theories, where a subset of Higgsings can be done via partial closing of punctures; fissions are precisely the Higgsings of class \mathcal{S} theories that are not given by partially closing punctures); and
- (iv) agreement with results in the mathematical literature, in particular, for symmetric products and affine Grassmannian slices.

C. The decay algorithm in practice

We now have described how to compute the Hasse diagram of the Coulomb branch of any good unitary quiver. The algorithm is very general and requires no input other

⁸Several examples of such nontrivial rebalancings are shown in Sec. III D 3.

⁹A reasonable guess, based on the first line of Table III, is that $\mu \cdot A_1$ should be extended to $\mu \cdot D_{g+1}$ for a genus $g \geq 2$ quiver.

than the initial quiver. However, it can be difficult to implement without the help of a computer, as the list of good subquivers to consider to build \mathcal{V} [see (2.7)] can be very large. Geometrically, it boils down to finding integral points in a convex cone in \mathbb{R}^n . In this subsection, we describe a convenient shortcut that applies to a class of simple quivers, namely, those for which only decay can occur, but never fission. This allows one to compute the diagrams efficiently by hand for these simple quivers.

Consider a quiver with unitary gauge nodes only, potentially nonsimply laced. Locate all the gauge nodes that have balance $b = 0$. These balanced connected subquivers take the form of a union of finite Dynkin diagrams.¹⁰ Assuming first that the quiver cannot fission into two good quivers, the decay transitions can, in practice, be implemented by the following subtractions¹¹:

- (1) A-type Kleinian singularity. For an overbalanced $U(k)$ node ($b > 0$), decay simply turns $U(k) \rightarrow U(k-1)$ and the transition is an A_{b+1} Kleinian singularity. This subtraction is only allowed if the quiver does not have any bad/ugly nodes ($b < 0$) after this subtraction.
- (2) Closure of minimal \mathfrak{g} orbit (one instanton). From a balanced, connected Dynkin-type subquiver, subtract the respective weighted finite Dynkin diagram of the Lie algebra \mathfrak{g} , see Table I. The transverse space of this transition is then the one- \mathfrak{g} instanton moduli space, provided there is no enhancement.
- (3) $h_{n,k}$ and $\bar{h}_{n,k}$ singularities. Suppose there exists a linear chain of $n-1$ balanced nodes on the short side of a k -laced edge that is connected to a node on the long side with balance b .
 - (a) For $b = k-2$, subtract the n node quiver $(1) - (1) - \dots - (1) \stackrel{k}{\leftarrow} (1)$ with a k -laced edge, such that the transverse slice is the $h_{n,k}$ singularity, see Table II.
 - (b) For $b = k-1$, subtract the n node quiver $(1) - (1) - \dots - (1) \stackrel{k}{\leftarrow} (1)$ with a k -laced edge such that the transverse slice is the $\bar{h}_{n,k}$ singularity, see Table II.

Note that not all the transverse slices obtained from decay that appear in this paper are of the types in (1)–(3). However, the algorithm is still sensitive to these other slices. If one performs the algorithm (1)–(3) and ends up with an ugly quiver, which contains a decoupled free hypermultiplet(s), the free hypermultiplet(s) enhance the transverse slice, for instance, into one of the more exotic slices in Table III.

¹⁰One can prove, by arguments similar to [57], that balanced (sub)quivers with unitary gauge groups need to take the shape of a finite Dynkin diagram.

¹¹In some talks given by Z. Z., this was previously called the “inverted quiver subtraction” algorithm.

TABLE I. Dynkin diagrams of classical and exceptional Lie algebras. The numbers at the nodes are the dual Coxeter labels.

	Classical algebras		Exceptional algebras
A_n		E_6	
B_n		E_7	
C_n		E_8	
D_n		F_4	
		G_2	

TABLE II. For both cases, the non-simply-laced quiver contains n $U(1)$ nodes, from which the first $n - 1$ are balanced and on the short side of the k -laced edge. The long $U(1)$ node has balance $b = k - 2$ and $k - 1$ for $h_{n,k}$ and $\bar{h}_{n,k}$, respectively.

$h_{n,k}$ and $\bar{h}_{n,k}$

The rules above provide a full list of decay products. One can then work out the possible fissions from there, by combining these decay products in all possible ways compatible with the original quiver.

D. A complete example

Now it is time to showcase the algorithm in an example that contains fission and decay, allows for a partial Higgsing interpretation, and can be compared to standard quiver subtraction (with all its subtleties).

As an example, consider the (electric) $SU(5)$ gauge theory¹² with $N_f = 4$ hypermultiplets in the fundamental representation and $N_{\Lambda^2} = 2$ hypermultiplets in the traceless second rank antisymmetric representation. Its magnetic quiver is given by¹³

(2.12)

As a first step, the decay and fission algorithm is applied to (2.12), which outputs the Hasse diagram in Fig. 5(a), which was displayed in the introductory cartoon of Fig. 1. The next step is to run the standard quiver subtraction algorithm on (2.12), which then results in the Hasse diagram in Fig. 5(b). As claimed above, the two Hasse diagrams agree, i.e., the same number of leaves and the same minimal transverse slices in between them. Moreover, the drastic difference in magnetic quivers obtained by the two algorithms becomes apparent. Fission and decay keeps the shape and reduces ranks at each step. In contrast, quiver subtraction forces us to include additional nodes due to rebalancing, requires decoration (here in green), or requires non-simply-laced edges.

The advantage of this example is that one can analyze branching rules for the $SU(5)$ gauge theory and directly follow the partial Higgs mechanism. Let us focus on the two transitions that the $SU(5)$ theory can undergo. There exists a partial Higgs mechanism

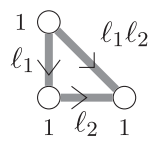
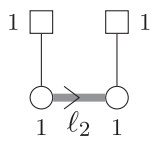
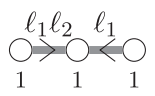
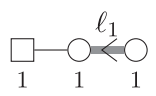
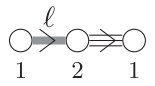
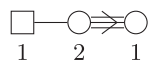
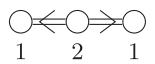
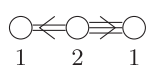
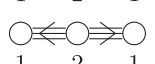
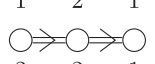
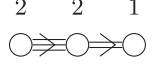
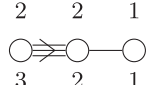
$$\begin{pmatrix} SU(5) \\ N_f = 4 \\ N_{\Lambda^2} = 2 \end{pmatrix} \longrightarrow \begin{pmatrix} SU(4) \\ N_f = 4 \\ N_{\Lambda^2} = 2 \end{pmatrix}, \quad (2.13)$$

which is straightforward in terms of branching rules $SU(5) \rightarrow SU(4)$,

$$[1, 0, 0, 0] \rightarrow [1, 0, 0] + [0, 0, 0] \quad (2.14a)$$

¹²For concreteness, consider this as a 3D $\mathcal{N} = 4$ theory.
¹³In spirit, this example is a truncated version of the magnetic quiver for the little string theory with an effective description given by an $\mathfrak{su}(5)$ gauge algebra supported on a curve of self-intersection 0, see [35]. In this example, the number of flavors is reduced to 4, which is well defined as 3D $\mathcal{N} = 4$ theory.

TABLE III. Complete list of good unitary quivers with three nodes or less whose Coulomb branch is an ICSS. The first column gives the raw results from the systematic search; the quivers are unframed and depend on a number of parameters, some of which may be redundant from the geometric perspective. The second column gives the framed version, which is not redundant. The geometry is given in the fourth column, and the way it is identified in the fifth. Dynkin diagram, DD. The second row from the bottom corresponds to a new singularity, discussed in the text.

Unframed	Framed	Condition	Geometry	Comments
U(2) with g adjoints	...	$g \geq 2$	D_{g+1}	[58]
		$n \geq 2, \ell \geq 1$	A_{n-1}	SQED quiver
	...	$\ell \geq 4$	$\mathcal{Y}(\ell)$	[29,50,59]
		$\ell_1, \ell_2 \geq 1$	\bar{h}_{2,ℓ_2}	[60]
		$\ell_1 \geq 2, \ell_2 \geq 1$	h_{2,ℓ_1}	[60]
		$\ell \geq 1$	g_2	Affine DD
	d_3	Twisted affine DD
	$\mathcal{J}_{2,3}$	[29]
	$\mathcal{J}_{3,3}$	[29]
	a_4	Twisted affine DD
	?	See text
	d_4	Twisted affine DD

$$[0, 1, 0, 0] \rightarrow [0, 1, 0] + [1, 0, 0] \quad (2.14b) \quad \left(\begin{array}{c} \text{SU}(5) \\ N_f = 4 \\ N_{\Lambda^2} = 2 \end{array} \right) \rightarrow \left(\begin{array}{c} \text{SU}(3) \\ N_f = 6 \end{array} \right) \otimes \left(\begin{array}{c} \text{SU}(2) \\ N_f = 4 \end{array} \right), \quad (2.15)$$

$$[1, 0, 0, 1] \rightarrow [1, 0, 1] + [1, 0, 0] + [0, 0, 1] + [0, 0, 0], \quad (2.14c)$$

where irreducible representations (IRs) are labeled by their Dynkin labels. This Higgsing is a decay in terms of the magnetic quiver (2.12) and is shown as the a_3 transition of (2.12) in Fig. 5(a). The “decay product” is, in fact, the magnetic quiver for the SU(4) gauge theory.

Additionally, there exists a partial Higgs mechanism of the form

which can be verified by inspecting branching rules $\text{SU}(5) \rightarrow \text{SU}(3) \times \text{SU}(2)$,

$$[1, 0, 0, 0] \rightarrow [1] \otimes [0, 0] + [0] \otimes [1, 0] \quad (2.16a)$$

$$[0, 1, 0, 0] \rightarrow [0] \otimes [0, 0] + [0] \otimes [0, 1] + [1] \otimes [1, 0] \quad (2.16b)$$

$$[1, 0, 0, 1] \rightarrow [0] \otimes [0, 0] + [2] \otimes [0, 0] + [0] \otimes [1, 1] + [1] \otimes [1, 0] + [1] \otimes [0, 1]. \quad (2.16c)$$

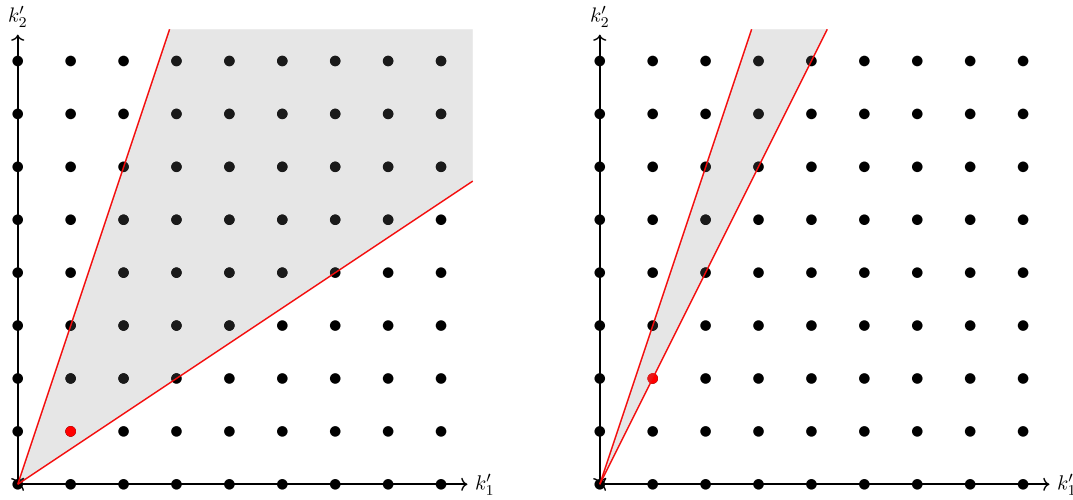


FIG. 6. Left: shape of the allowed (k'_1, k'_2) region in a situation where $a \geq 2$ and $b \geq 1$ (here $a = 3$ and $b = 2$). Right: shape of the allowed (k'_1, k'_2) region in a situation where $a = 1$ and $b \geq 4$ (here $b = 6$). In both cases, the unique minimal nonzero quiver is the red dot.

The reason why the $SU(5)$ theory splits into a direct product is that the IRs $[1] \otimes [1, 0] + [1] \otimes [0, 1]$, charged under both gauge group factors, precisely cancel between the decomposition of the adjoint and the second antisymmetric (and its complex conjugate). From the magnetic quiver perspective, this Higgsing is the A_1 fission of (2.12) in Fig. 5(a). The two “fission fragments” are indeed the magnetic quivers for the $SU(3)$ and $SU(2)$ gauge theory, respectively.

Continuing this branching analysis yields the Higgs branch Hasse diagram in Fig. 5(c). Comparing to Fig. 5(a) demonstrates that all quivers obtained via the decay and fission algorithm are the magnetic quivers for the (electric) theories obtained from the partial Higgs mechanism. In the next section, a host of examples is detailed. For most of them, one does not have a weakly coupled description such that Higgs branch RG flows are substantially more involved than a vanilla partial Higgs mechanism. The decay and fission algorithm then offers a unique approach to analyze the possible Higgs branch RG flows in a systematic way.

E. Classification of isolated singularities

The algorithm presented in Sec. II C can be used to identify quivers whose Coulomb branch is an *isolated* conical symplectic singularity (ICSS). In practice, this amounts to classifying pairs (A, K) such that the set of leaves (2.10) contains exactly two elements (the trivial leaf, i.e., the singularity, and the nontrivial leaf). This is a well-defined mathematical question, which can presumably be addressed abstractly, thereby providing a full classification. We postpone this for future work, but we present here a first step in that direction, by using a brute force approach that is applicable to quivers with a small number of nodes. Specifically, we focus on quivers with $n = 1, 2, 3$ nodes.

The case $n = 1$ is essentially trivial: the matrix A reduces to an even integer $A \geq -2$. If $A = -2$, no good quiver can be constructed. If $A \geq 0$, every quiver with $K \geq 2$ gives a nontrivial singularity, and whenever $K \geq 3$, the quiver can fission or decay. Therefore, the $n = 1$ case corresponds to the family of quivers $(A, K) = (2g, 2)$, or in other words, $U(2)$ with $g - 1$ adjoint hypermultiplets.

Let us move on to $n = 2$. We can restrict to the case where there are no loops, i.e., $A_{1,1} = A_{2,2} = -2$. By symmetry, we can parametrize the quivers as

$$(A, K) = \left(\begin{pmatrix} -2 & a \\ ab & -2 \end{pmatrix}, (k_1, k_2) \right) \tag{2.17}$$

with $k_1, k_2, a, b \in \mathbb{Z}_{>0}$. The conditions \mathcal{P}_1 and \mathcal{P}_2 are never satisfied by (2.17), so the set \mathcal{V} is defined as the set of pairs $(k'_1, k'_2) \in \mathbb{N}^2$ such that $k'_1 \leq k_1, k'_2 \leq k_2$ and

$$-2k'_1 + ak'_2 \geq 0, \quad abk'_1 - 2k'_2 \geq 0. \tag{2.18}$$

For there to be a solution, it is necessary that $a^2b \geq 4$. This leads to two types of solutions, as illustrated in Fig. 6:

- (i) $a \geq 2$ and $b \geq 1$. In this case, $(k'_1, k'_2) = (1, 1)$ satisfies (2.18) and is minimal, which gives the quiver

$$\begin{array}{ccc} & a, b & \\ & \circ \rightleftarrows \circ & \\ & 1 \quad \quad 1 & \end{array} \tag{2.19}$$

This corresponds to the A_{a-1} singularity.

- (ii) $a = 1$ and $b \geq 4$. Now $(k'_1, k'_2) = (1, 2)$ satisfies (2.18) and is minimal, which gives the quiver

$$\begin{array}{c} \textcircled{b} \\ \textcircled{2} \rightarrow \textcircled{1} \end{array} \quad (2.20)$$

This corresponds to the $\mathcal{Y}(b)$ singularities.

Finally, we can similarly analyze the $n = 3$ case, using similar—but much longer—arguments. All in all, we finally obtain the list shown in Table III. It is interesting

to note that almost all the quivers that emerge from this study have been studied in the literature, although very recently for some of them, see the comment column in Table III. However, we find one outlier (the shaded row in the table) for which we believe the geometry has not been studied. It has isometry $\mathfrak{sp}(2)$ and the Coulomb branch Hilbert series (HS) reads

$$\begin{aligned} \text{HS}(t) &= \frac{1 + 4t^2 + 31t^4 - 7t^6 + 22t^8 - 102t^{10} + 22t^{12} - 7t^{14} + 31t^{16} + 4t^{18} + t^{20}}{(-1 + t^2)^8(1 + t^2)^2(-1 + t^4)^2} \\ &= 1 + 10t^2 + 80t^4 + 359t^6 + 1295t^8 + 3751t^{10} + 9560t^{12} + 21675t^{14} + 45313t^{16} + O(t^{18}). \end{aligned} \quad (2.21)$$

The highest weight generating function reads [in conventions where α_1 is the short simple root and α_2 is the long simple root of $\mathfrak{sp}(2)$]

$$\begin{aligned} \text{PE}[\mu_1^2 t^2 + (1 + \mu_2^2 + \mu_2^3) t^4 + \mu_2^3 t^6 - \mu_2^6 t^{12}] &= 1 + \mu_1^2 t^2 + (\mu_1^4 + \mu_2^3 + \mu_2^2 + 1) t^4 \\ &+ (\mu_1^6 + \mu_2^3 \mu_1^2 + \mu_2^2 \mu_1^2 + \mu_1^2 + \mu_2^3) t^6 + O(t^7). \end{aligned} \quad (2.22)$$

where PE is Plethystic Exponential.

Two natural questions then arise from this study: First, can this new quiver be obtained from a brane construction or geometric engineering in string theory? And second, can one generalize this search to arbitrary number of nodes? We leave these fundamental challenges for future work and turn now to applications of our algorithm to various physical situations.

III. DECAY AND FISSION IN ACTION: SELECTED EXAMPLES

We now apply the decay and fission algorithm on selected examples in space-time dimensions $d = 3, 4, 5, 6$. This case study illuminates and demonstrates the arising Higgsing pattern between different theories.

A. 3D $\mathcal{N} = 4$ theories

1. Intuition via mirror symmetry

In this subsection, we consider a class of 3D $\mathcal{N} = 4$ theories for which one can directly use 3D mirror symmetry in order to prove the validity of the decay algorithm (no fission occurs here). In this specific framework, there is a duality between decay and the quiver subtraction of [5]: one corresponds to moving on the Higgs branch, while the other corresponds to moving on the Coulomb branch.

Higgs and Coulomb branch Higgsing. Consider a Lagrangian gauge theory, with some scalars transforming in a representation R of the gauge group G . The scalars may acquire nontrivial VEVs, which breaks the gauge group to a subgroup H . Depending on the type of the residual gauge

group, the phases in a given vacuum carry different names. For example, for R the fundamental representation H is a subgroup of G with reduced rank—these are called Higgs vacua, in analogy to the Standard Model. On the other hand, for R the adjoint representation H is a subgroup of G with the same rank (adjoint Higgsing)—these are called Coulomb vacua, because H , in general, contains $U(1)$ factors.

A large class of 3D $\mathcal{N} = 4$ theories have two maximal branches of the moduli spaces of supersymmetric vacua: the Higgs and Coulomb branches, which are parametrized by VEVs of scalar fields in hypermultiplet and vector multiplets, respectively. Consequently, there are two types of Higgs mechanisms: one triggered by a VEV for a hypermultiplet scalar and the other triggered by a VEV for a vector multiplet scalar—in short, a Higgs or Coulomb branch Higgs mechanism, respectively.

To gain intuition, consider the linear quiver gauge theories $T_\rho^\sigma[\text{SU}(N)]$. Higgs branch (HB) Higgsing can be effectively realized on the quiver theory by the following:

- (HB1) Mesons of a single gauge: subtracting the supersymmetric QED (SQED) with N flavors quiver $(1) - [N]$ from the gauge node. Here, the single gauge node $U(k) \rightarrow U(k - 1)$ is partially broken.
- (HB2) Gauge invariant spanning several gauge nodes: subtracting the linear quiver $[1] - (1) - \dots - (1) - [1]$ between two flavor nodes. Here, a whole sequence of gauge group factors $U(k_i) \rightarrow U(k_i - 1)$ is partially broken.

To illustrate, consider the partial Higgs mechanisms along the Higgs branch in Fig. 7(a). Note, in particular, that the

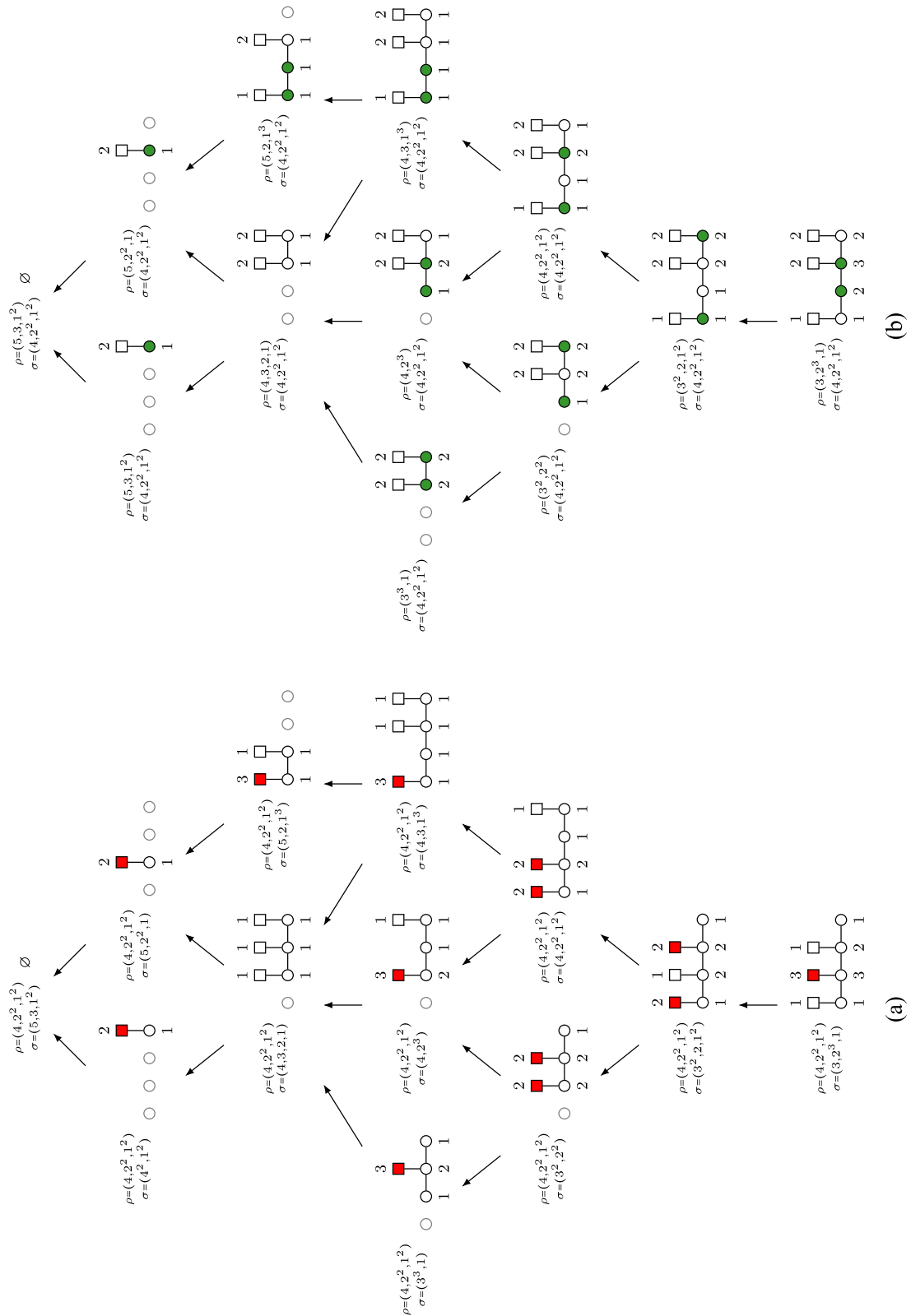


FIG. 7. (a) Partial Higgs mechanism of a theory $\mathcal{T} = T_\rho^\sigma[\text{SU}(10)]$ with $\rho = (4, 2^2, 1^2)$, $\sigma = (3, 2^3, 1)$ and (b) its mirror $\mathcal{T}^\vee = T_\sigma^\rho[\text{SU}(15)]$. The red colored flavor nodes indicated non-Abelian global symmetries that trigger minimal Higgs branch transitions. On the mirror, this translates to the set of balanced nodes indicated by green. At each step, mirror symmetry is manifest via exchanging $\rho \leftrightarrow \sigma$.

balance of the gauge nodes is preserved during Higgs branch Higgsing, which is evident from the D3-D5-NS5-brane configurations [61]. In terms of quiver subtraction, this is known as the rebalancing condition after the subtraction and leads, in general, to a change of flavor nodes. On a related note, there exists an algorithm in the mathematics literature [62–64] that produces these quivers for the Higgs branch Higgsing. Related to decay via 3D mirror dual, this algorithm also shares a remarkable feature in that it defines a quiver via the adjacency matrix A and a rank vector K , and subsequently generates quivers for each leaf of the Higgs branch.

On the mirror side (or in terms of magnetic quivers), these Higgs branch transitions are partial Higgs mechanisms along the Coulomb branch. Since the flavor nodes have been the indicator for the Higgs branch transitions (because Higgs branch gauge invariant operators need to start and end at flavor nodes), the topological symmetry (i.e., the balance of the gauge nodes) is the smoking gun for Coulomb branch Higgs transitions. Again, this is particularly transparent in the brane realization. On the level of the quiver theory, Coulomb branch (CB) Higgsing has equally straightforward implementation [65]:

- (CB1) For a connected set of balanced gauge nodes, Coulomb branch Higgsing breaks all nodes partially: $U(k_i) \rightarrow U(k_i - 1)$, but the flavor nodes are not affected. This can be realized by subtracting the finite weighted A -type Dynkin quiver $(1) - (1) - \dots - (1)$.
- (CB2) For an overbalanced node, not connected to any balanced nodes, Coulomb branch Higgsing only breaks this gauge group factor via $U(k) \rightarrow U(k - 1)$. On the quiver, one simply subtracts a (1) node.

This is exemplified in Fig. 7(b). In contrast to Higgs branch transitions, the partial Higgs mechanisms CB1 and CB2 do not preserve the balance of the gauge nodes.

The point to appreciate is the following: given a theory \mathcal{T} that admits a Higgs branch transition HB1 or HB2 to \mathcal{T}_1 , then, assuming that the mirror theory of \mathcal{T} is \mathcal{T}^\vee , the mirror of \mathcal{T}_1 is simply obtained from \mathcal{T}^\vee by either CB1 or CB2.

It is a simple exercise to generalize the rule CB1 for Coulomb branch Higgsing to other unitary quiver theories, such as BCD -type Dynkin quivers, see [65]. Using, for instance, O5 or ON planes, one deduces that also weighted finite Dynkin diagrams of type BCD can be subtracted. As a result, CB1 and CB2 motivate the practical implementation (1 and 2), which in turn can be interpreted in terms of decays.

Magnetic quivers and decay transitions. As an example, consider the theory $\mathcal{T} = T_\rho^\sigma[\text{SU}(10)]$ with $\rho = (4, 2^2, 1^2)$, $\sigma = (3, 2^3, 1)$. The Higgsings on the Higgs and Coulomb branches are shown in Fig. 7. The quiver subtraction algorithm generates magnetic quivers $\mathbf{Q}^{\mathcal{L}_i}$ for the closure

of each leaf $\tilde{\mathcal{L}}_i$ in the stratification of the Higgs branch of \mathcal{T} . However, *none* of these $\mathbf{Q}^{\mathcal{L}_i}$ are the magnetic quiver for any of the theories \mathcal{T} can be Higgsed to, i.e., the quivers in Fig. 7(a). In contrast, directly utilizing the decay algorithm [Fig. 8(a)] generates a different set of quivers $\mathbf{Q}_{\mathcal{L}_i}$. These *are* the magnetic quivers for the different theories \mathcal{T}_i that can be obtained from \mathcal{T} via partial Higgsing along the Higgs branch [Fig. 7(a)]. The special feature in 3D $\mathcal{N} = 4$ is

$$\mathbf{Q}_{\mathcal{L}_i} = (\mathcal{T}_i)^\vee, \quad (3.1)$$

meaning that the magnetic quivers $\mathbf{Q}_{\mathcal{L}_i}$ obtained from the decay and fission algorithm are, in fact, the mirror theories of the \mathcal{T}_i themselves. This is evident from our example in Figs. 7(b) and 8(a).

Framed vs unframed quivers. A magnetic quiver is typically represented as an unframed quiver (without flavor nodes). In cases where all the gauge groups are unitary (which is always the case in this paper), this implies that there is an overall $U(1)$ that decouples from the theory. Choosing to decouple this $U(1)$ from a $U(1)$ gauge group creates flavor nodes, thereby framing the quiver. In instances like the $T_\rho^\sigma[\text{SU}(N)]$ family, applying the decay and fission algorithm to either the unframed (Fig. 8) or framed version (Fig. 7) of the magnetic quivers yields the same result. However, this is not generally the case, and only by considering unframed magnetic quivers can we capture all the Higgsings without missing any.¹⁴

2. Mixed U/SU quivers

Figures 7(b) and 8(a) illustrate the application of the decay and fission algorithm on a pair of quivers belonging to the $T_\rho^\sigma[\text{SU}(N)]$ family. This family, a broad spectrum of quiver theories, was initially introduced in [66] and is characterized by the mirror pairs being linear quivers with unitary gauge groups. The $T_\rho^\sigma[\text{SU}(N)]$ family was further generalized in [67] to accommodate linear quivers with an assortment of both unitary and special unitary gauge groups. This expansion significantly broadened the repertoire of recognized 3D mirror pairs. Regarding these U/SU quivers, which we represent as $T_\rho^\sigma[\text{SU}(N)]_{U/SU}$, the 3D mirrors continue to consist solely of unitary gauge groups. However, it should be noted that the mirrors no longer conform to the linear quiver structure. The $T_\rho^\sigma[\text{SU}(N)]_{U/SU}$ represents a Lagrangian theory where Higgsings can be conducted utilizing group theoretic analysis, as outlined in [5]. However, due to the incorporation of special unitary

¹⁴It is possible to only work with framed quivers, one just needs to consider *all* the different choices of $U(1)$ decoupling when performing the subtraction.

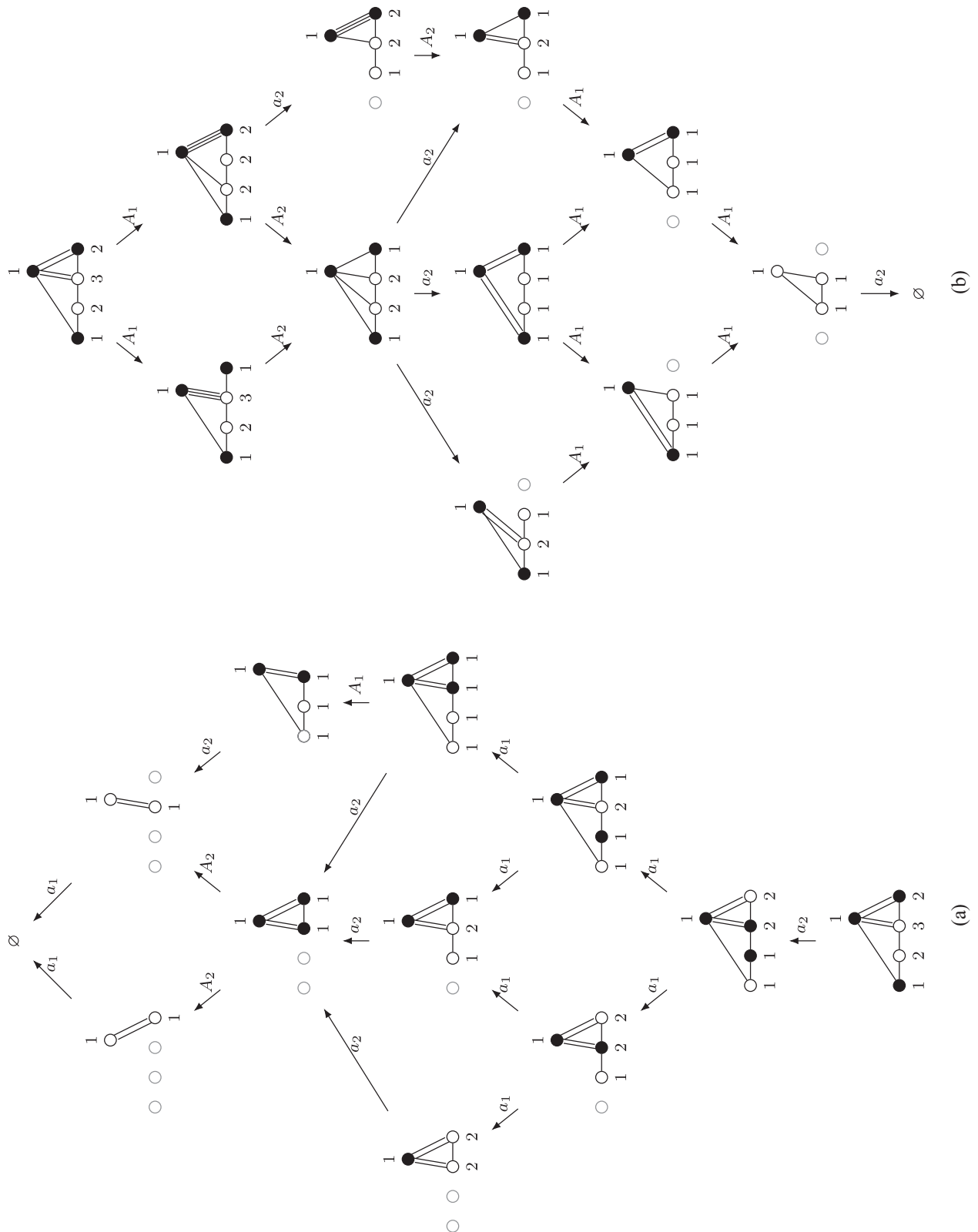
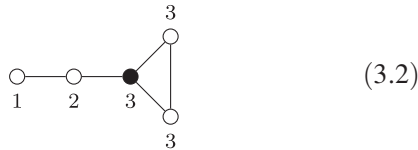


FIG. 8. Comparison of (a) the decay algorithm and (b) quiver subtraction. White nodes are balanced, black nodes are overbalanced. Note that, for 3D $\mathcal{N} = 4$ gauge theories, Coulomb branch Higgsing on a framed quiver \mathbf{Q} is identical to the decay (and fission) algorithm on the unframed version of \mathbf{Q} . In other words, compare Figs. 7(b) and 8(a).

gauge groups, this procedure becomes significantly more complex, as evidenced by the intricate Hasse diagrams detailed in [67]. Despite these complexities, the 3D mirror of the $T_\rho^\sigma[\text{SU}(N)]_{U/SU}$ consists entirely of unitary quivers, thus allowing us to once again implement the decay and fission algorithm. The quivers, after decays, can be mapped back to members of the $T_\rho^\sigma[\text{SU}(N)]_{U/SU}$ theories, using the algorithms provided in [67], giving us the Higgsing tree. A proof of concept is given in Fig. 9.

3. Fission

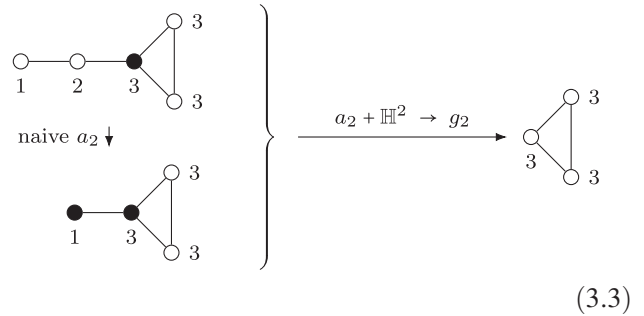
To illustrate all aspects of decay and fission, and to motivate the introduction of the condition \mathcal{P}_2 in (2.7), consider the following quiver:



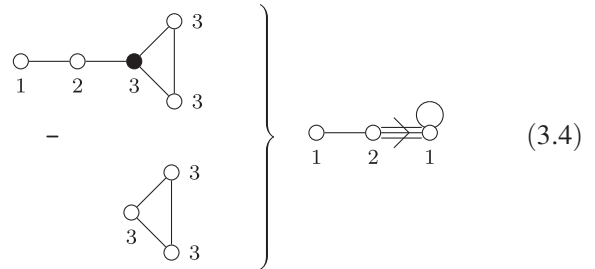
for which the decay and fission algorithm produces the Hasse diagram shown in Fig. 10(a). For comparison, the Hasse diagram obtained via quiver subtraction is compiled in Fig. 10(b). A visual inspection confirms two facts: First, the transverse slice geometries associated with minimal transitions are identical in both algorithms. Second, the magnetic quivers obtain in both algorithms are substantially different. Let us now comment on the phenomena in more detail.

In the decay algorithm, the general idea is to list all quivers of the same shape, but with smaller rank vector. However, in certain specific cases, such a quiver can still contain free hypermultiplets. The most well-known example is a $U(1)$ attached to an n -stacked affine Dynkin diagram of algebra \mathfrak{g} , such as (3.2). The resulting moduli space is the $n - \mathfrak{g}$ instanton moduli space, plus a free hypermultiplet. However, rather than decaying to a theory with a decoupled free hypermultiplet, we expect the free hypermultiplet to enhance (or possibly fibrate) the transverse slice in between instead. This is the essence of condition \mathcal{P}_2 in (2.7).

Returning to (3.2) and recalling the practical implementation (1–3), the two decays are the a_2 coming from the left two balanced nodes and the a_2 from the right two balanced nodes. However, the naive a_2 decay in the left nodes would lead to the quiver of the three- $SU(3)$ instantons on \mathbb{C}^2 . This contains a free \mathbb{H} factor and is excluded in the decay algorithm, as discussed above. Thus, the complete algorithm step is simply



and the transverse slice is obtained as described in Sec. II B. One finds



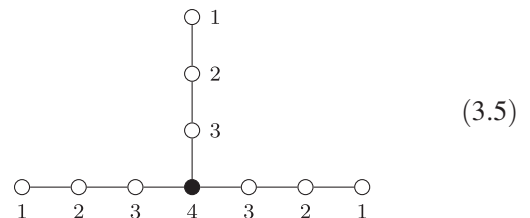
which yields a g_2 slice due to the non-simply-laced rebalancing with $\text{gcd} = 3$.

B. 4D $\mathcal{N} = 2$ theories

The landscape of 4D $\mathcal{N} = 2$ theories accommodates a host of non-Lagrangian theories; see [68–74] and subsequent works. For those, the partial Higgs mechanisms (or Higgs branch RG flows) are far from obvious and we demonstrate that the decay and fission algorithm is a powerful technique to trace out the entire Higgs branch Hasse diagram.

1. Class \mathcal{S} theories

A large class of 4D $\mathcal{N} = 2$ SCFTs is generated using the class \mathcal{S} framework. In this case, the decay and fission algorithm reproduces the Higgsing from one theory to the next by partially closing punctures. Let us consider as a simple example the T_4 theory. It can be constructed as a class \mathcal{S} theory labeled by a punctured Riemann surface [66] with three maximal punctures. Its magnetic quiver reads [75]



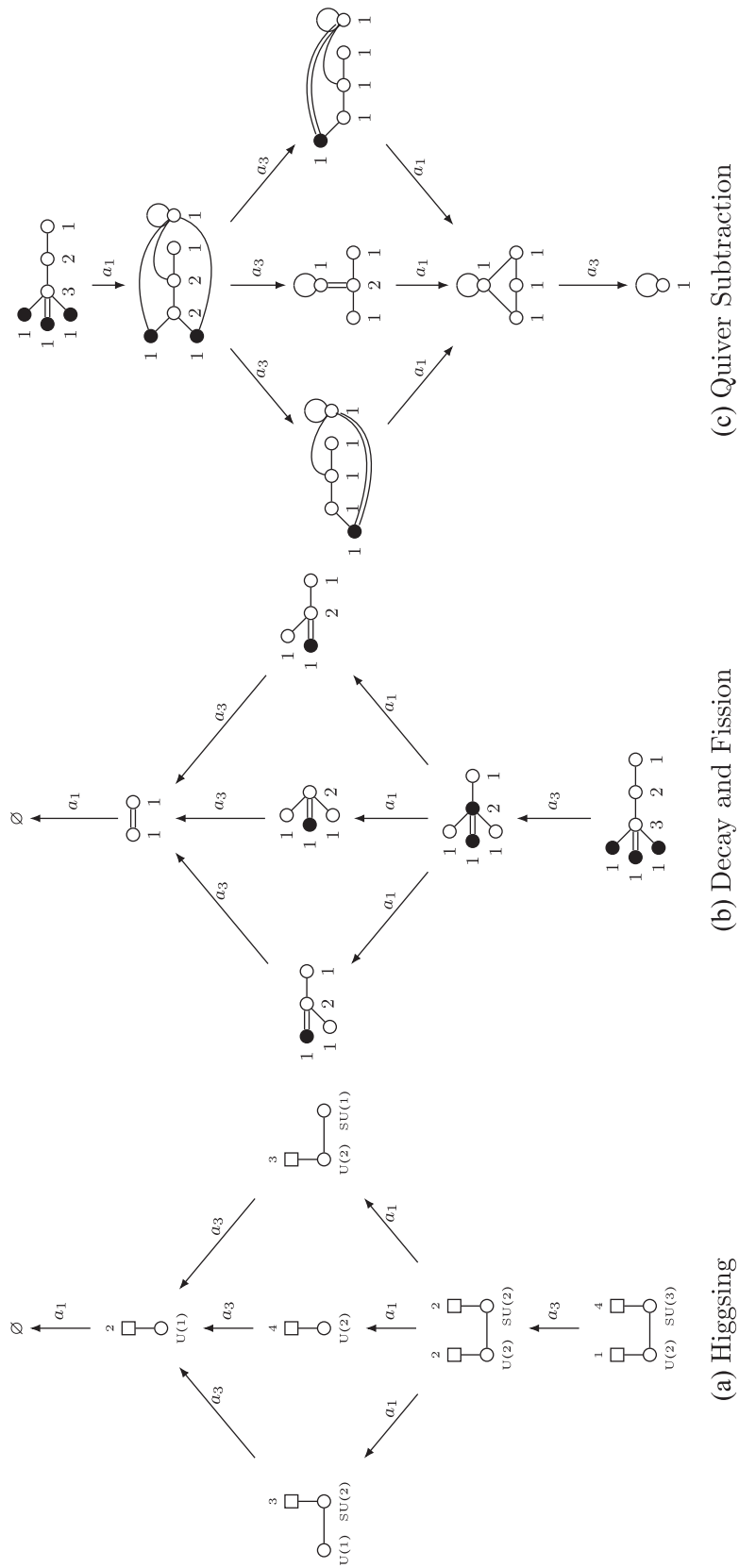


FIG. 9. Example for a mixed U/SU quiver. (a) Displays the partial Higgsing pattern of the (electric) U/SU quiver with $U(2) \times SU(2)$ gauge group. (b) Derives the Higgsing pattern from the decay and fission algorithm starting from the magnetic quiver. (c) Provides a comparison with quiver subtraction.

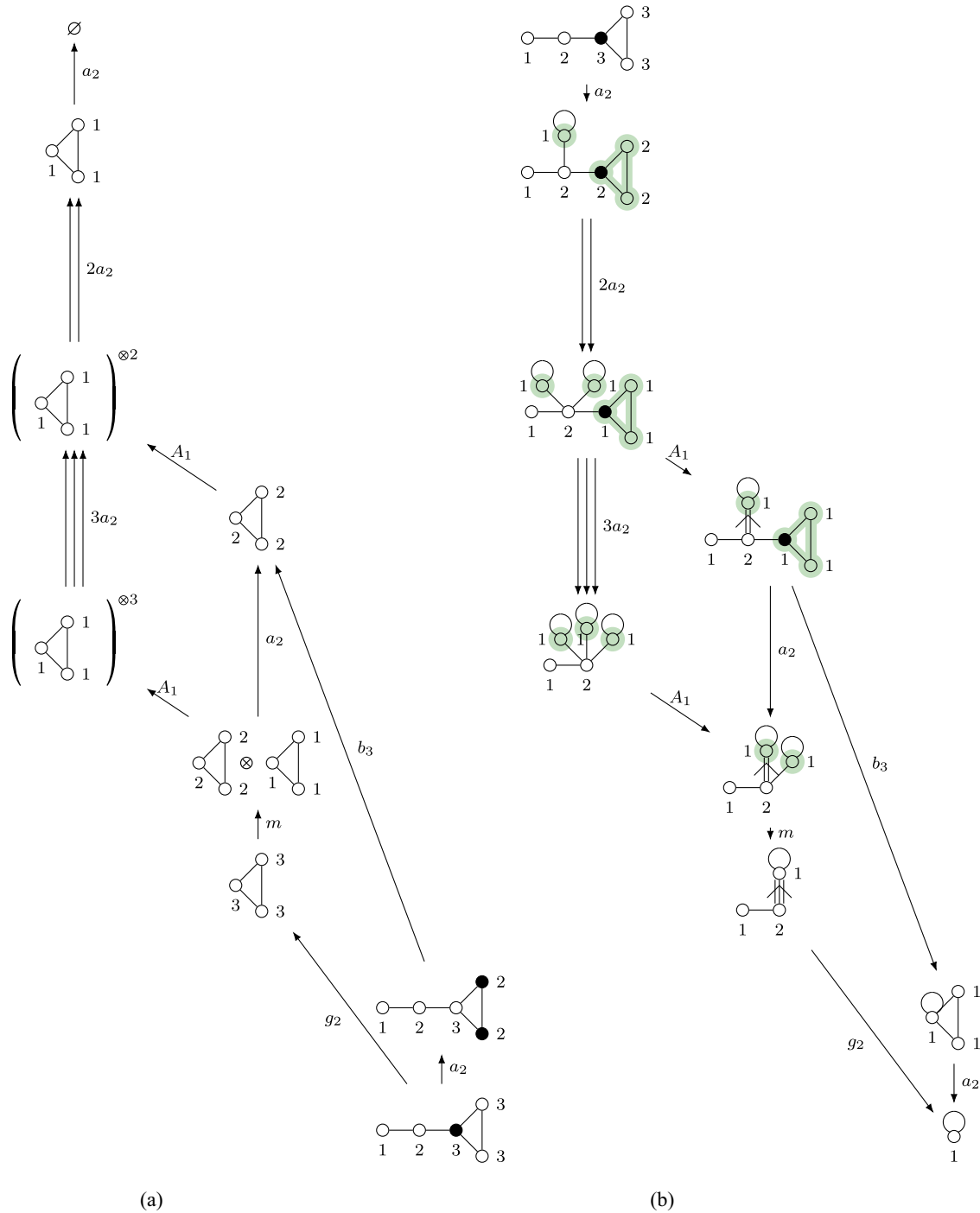


FIG. 10. Hasse diagram of the magnetic quiver (3.2). (a) Via decay and fission algorithm. (b) Via quiver subtraction, wherein green indicates decoration. Note that fission reproduces all the transverse slices that are unions, e.g., $3a_2 = a_2 \cup a_2 \cup a_2$.

and applying the decay and fission algorithm results in the Hasse diagram shown in Fig. 11(a). For comparison, the quiver subtraction result is shown in Fig. 11(b).

As advertised in the Introduction, the algorithm indeed generalizes the closing of punctures in the class \mathcal{S} language; to see this, it is useful to translate Fig. 11 into a Higgsing pattern of 4D SCFTs, shown in Fig. 12.

The a_3 decay transition partially closes a regular puncture $(1^4) \rightarrow (2, 1^2)$ and realizes the Higgsing of $T_4 \rightarrow R_{0,4}$. Similarly, the subsequent a_1 decay is the further closure of the puncture $(2, 1^2) \rightarrow (2^2)$ and realizes the $R_{0,4} \rightarrow MNE_7$ Higgsing. However, the Higgsing $R_{0,4} \rightarrow MNE_6$ involves changing the rank of class \mathcal{S} theory from A_3 to A_2 which is more involved than just partially closing a

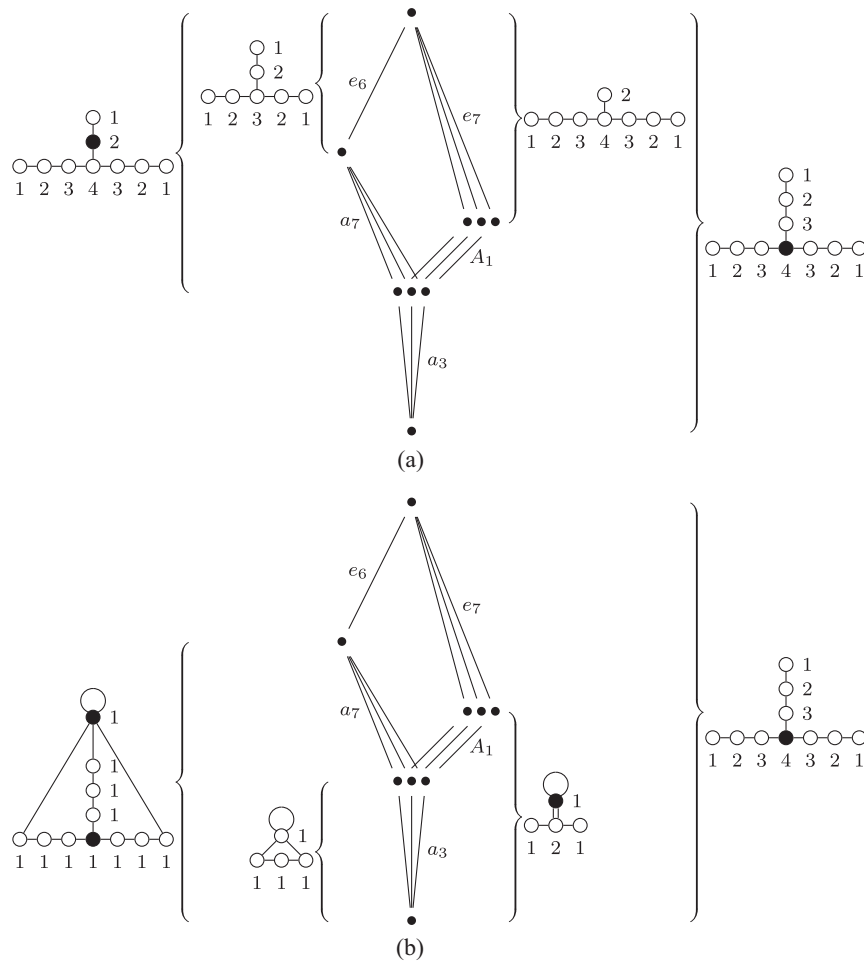


FIG. 11. The (a) decay algorithms and (b) quiver subtraction for the T_4 magnetic quiver generate two sets of quivers. The Coulomb branches of these quivers are equivalent to the transverse spaces between the symplectic leaves (dots) indicated by the brackets in the Hasse diagram.

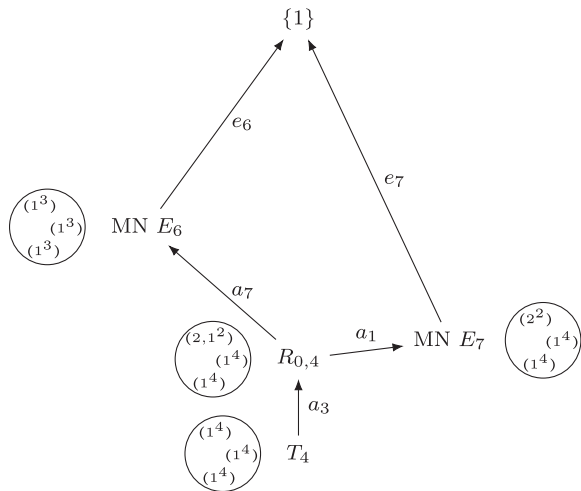


FIG. 12. Higgsing pattern relating 4D $\mathcal{N} = 2$ theories starting from T_4 . E_6 , E_7 denote the Minahan-Nemeschansky (MN) theories. Note that, in contrast to Fig. 11, the equivalent transitions are not displayed, due to symmetry.

puncture.¹⁵ Furthermore, fission is not covered by closing partial punctures; this is particularly evident when the quiver contains stacks of affine Dynkin subquivers. We conclude that, even for class \mathcal{S} theories, the closing of a partial puncture does not realize all possible Higgsings.

2. Argyres-Douglas theories

One can also consider Argyres-Douglas (AD) theories [70], which are constructed in class \mathcal{S} making use of irregular punctures [76]. The magnetic quivers of these

¹⁵This Higgsing can be done as follows. First, partially closing one of the punctures leads to a magnetic quiver where one of the gauge nodes has balance -1 . This means the quiver contains some free hypermultiplets that need to be removed. One then needs to do a set of Seiberg dualities to ensure all the nodes have positive balance. The resulting quiver is the magnetic quiver of the Higgsed theory, which can then be mapped back to the MNE_6 . In general, this step of performing Seiberg dualities on all the nodes makes the Higgsing procedure much more inefficient and can often lead to a nonminimal Higgsing.

The pattern of partial Higgsing of the $D_9\text{SU}(6)[1^6]$ theory obtained from the decay and fission algorithm is summarized in Fig. 13.

To begin with, let us analyze the decays. The Higgsings for $(A_2, A_5)[\rho]$, with ρ a partition of 6, can be understood as closing the regular puncture, which changes the partitions and, in turn, shortens the tail of the magnetic quiver. However, the transitions like the A_7 or A_9 decay are achieved by removing one of the overbalanced $U(1)$ gauge nodes in the complete graph.¹⁶ This decay can be interpreted as Higgsing the irregular puncture which changes its nature from (A_2, A_5) to (A_1, A_3) . The resulting AD theories are $(A_1, A_3)[1^4]$ and $(A_1, A_3)[2^2]$, respectively. Thus, we see from the decay point of view that the Higgsing of the irregular puncture is naturally captured as well.

Crucially, the irregular puncture also triggers fissions, due to the presence of highly overbalanced nodes in the complete graph. These transitions are depicted in red in Fig. 13.

For AD theories with more than one regular puncture, e.g., [77], the same Higgsing process can be done as long as the magnetic quiver is made of only unitary gauge groups. For some 4D SCFTs, it is well known that they may not be completely Higgsable. Therefore, in such cases, the top of the Higgsing diagram where we denote the theory with $\{1\}$ really refers to an SCFT with a trivial Higgs branch rather than a trivial theory.

3. SCFTs with non-simply-laced magnetic quivers

As shown, for example, in the exhaustive lists of [11,21], magnetic quivers for 4D $\mathcal{N} = 2$ SCFTs are often non-simply laced, and the decay and fission algorithm applies in

this case as well. For instance, consider the following quiver:

$$\begin{array}{c} \circ - \circ - \circ - \circ - \bullet \\ 1 \quad 2 \quad 3 \quad 4 \quad 5 \end{array} \quad (3.7)$$

which is the magnetic quiver [11] of a rank-2 4D $\mathcal{N} = 2$ SCFT introduced in [80], labeled as $Q_{A_3}^2$, as it is part of the $Q_{A_3}^n$ family of SCFTs, or labeled $\mathfrak{su}(5)_{16}$ in [21,42]. Using the decay and fission algorithm, the arising Higgsing pattern between 4D $\mathcal{N} = 2$ SCFTs can be summarized as in Fig. 14.

Applying the decay and fission algorithm to the rank 3 SCFT $Q_{A_3}^3$ in the same family, one obtains Fig. 15(a), which translates into a Higgsing pattern between 4D SCFTs as shown in Fig. 15(b).

4. An \mathcal{S} -fold theory: Multiple affine Dynkin diagrams

Consider the theory $\mathring{T}_{A_2,2}^{r=3}$ introduced in [17]. This theory is an orbifold of \mathcal{S} -fold theories with the following magnetic quiver:

$$\begin{array}{c} \bullet \\ \parallel \\ \bullet \\ \diagup \quad \diagdown \\ \circ \quad \circ \\ 1 \quad 3 \quad 3 \end{array} \quad (3.8)$$

One observes a stack of three a_2 affine Dynkin diagrams. This signals the possibility of fission. The full diagram can be obtained by running the algorithm; we do not present it here, but focus on the bottom part, which shows four possible Higgsing transitions as follows:

This analysis shows that the magnetic quiver (3.8) admits two decay and two fission transitions; hence, the \mathcal{S} -fold theory $\mathring{T}_{A_2,2}^{r=3}$ should admit four distinct Higgs branch RG flows,

¹⁶Naturally, there are three equivalent A_7 or A_9 decays and we only wrote down one of them to prevent cluttering the diagram.

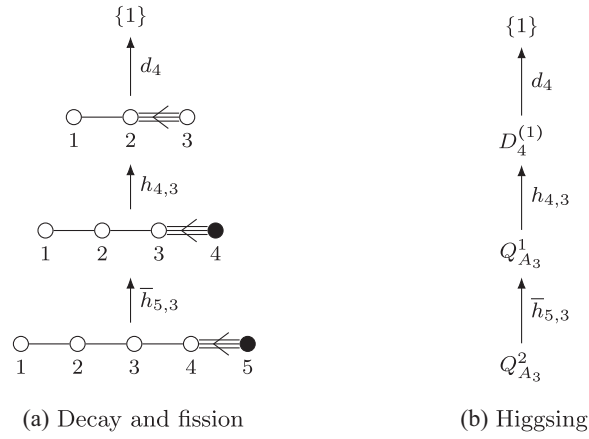


FIG. 14. (a) Magnetic quivers from the decay algorithm. (b) Higgsing pattern of the $Q_{A_3}^2$ SCFT. Here, $Q_{A_3}^1$ labels an $\mathcal{N} = 2$ SCFT with Higgs branch global symmetry A_3 [11] and $D_4^{(1)}$ is a 4D SCFT with Higgs branch being the one-SO(8) instanton moduli space.

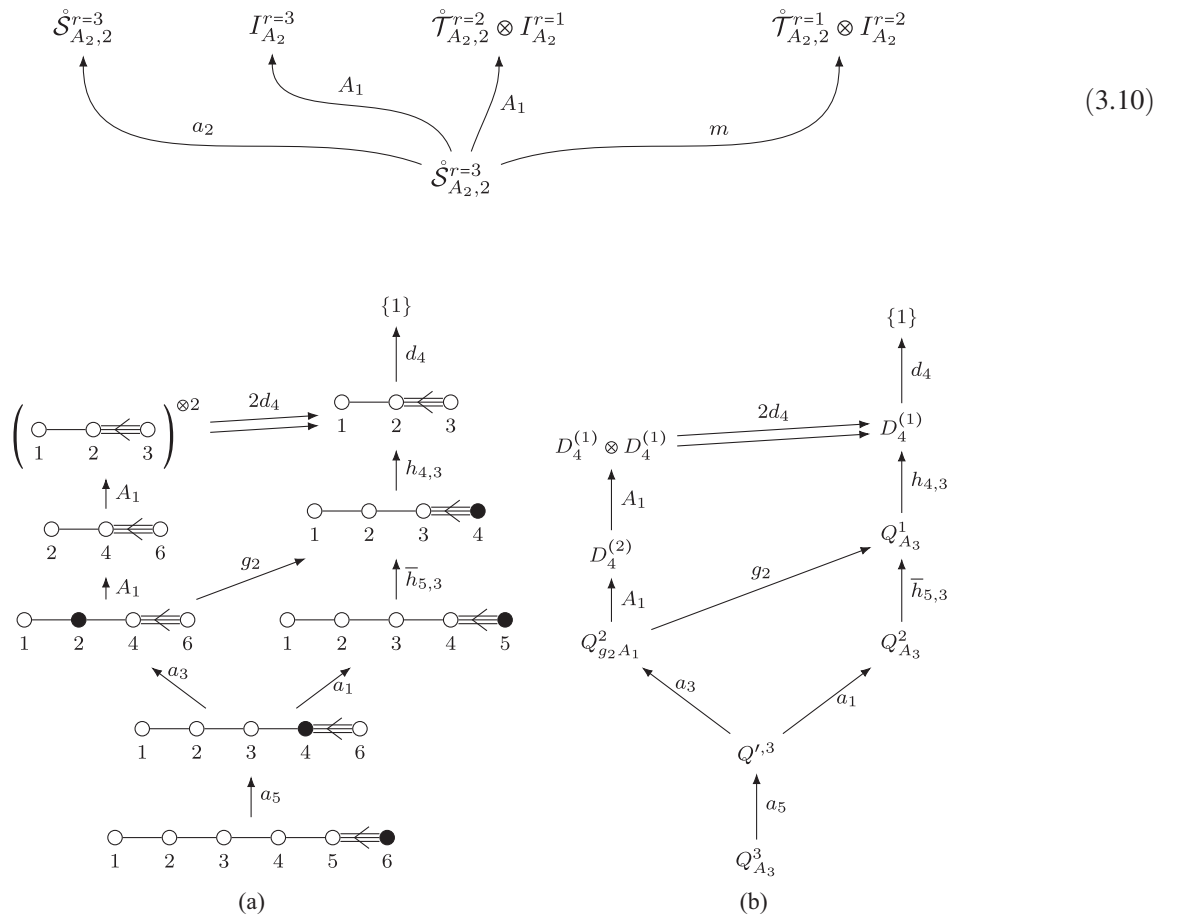


FIG. 15. (a) Decay and fission algorithm on the magnetic quiver of $Q_{A_3}^3$. (b) The Higgsings between 4D SCFTs. Here $Q_{g_2 A_1}^2$ is a rank-2 SCFT introduced in [81]; its Higgs branch global symmetry is $\mathfrak{g}_2 \times \mathfrak{su}(2)$. The transition $Q_{g_2 A_1}^2 \rightarrow D_4^{(1)} \otimes D_4^{(1)}$ was conjectured in [17] to be k_3 . However, we conjecture that k_3 is not an elementary transition, but rather composed of two consecutive A_1 transitions. The fission $D_4^{(2)} \rightarrow D_4^{(1)} \otimes D_4^{(1)}$ is analogous to the example in Sec. II A; where $D_4^{(2)}$ is the rank-2 SCFT with Higgs branch being the two-SO(8) instanton moduli space. The second magnetic quiver from the bottom in 15(a) has not yet been matched with a 4D theory. This is likely because the theory is a rank-3 4D theory, which is not yet classified. The candidate 4D theory has $\mathfrak{su}(4) \times \mathfrak{su}(2)$ global symmetry and is labeled as Q'^3 .

which completes the preliminary results of Fig. 12 in [17]. The $\mathcal{S}_{G,\ell}^r$ theories are another type of \mathcal{S} -fold theories, and I_G^r denotes the r G instanton theories. Working out the entire Hasse diagram produces 21 symplectic leaves in total. This is straightforward, and they are not detailed here.

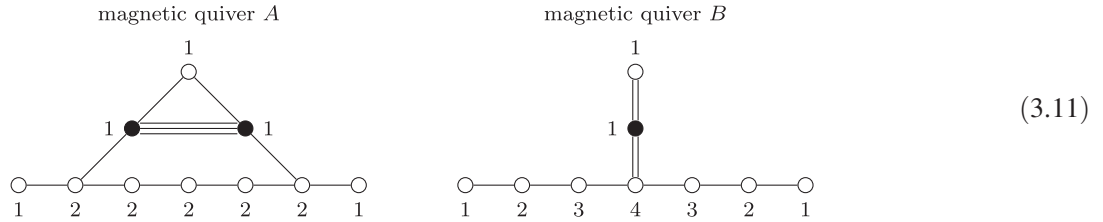
C. 5D $\mathcal{N} = 1$ theories

In this section, we consider partial Higgsing of 5D SCFTs which can be deformed to supersymmetric QCD theories with $SU(N_c)_{|k|}$ with N_f fundamental flavors, N_{Λ^2}

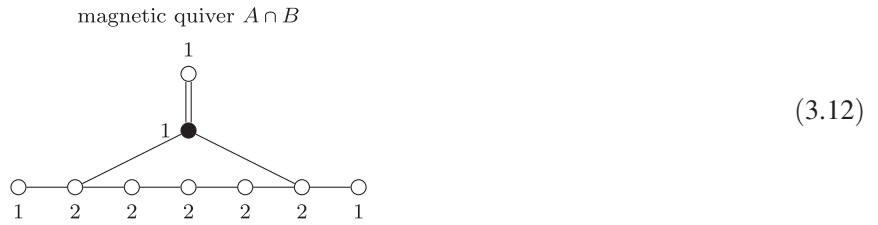
antisymmetrics, and Chern-Simons levels k . The magnetic quivers of these theories have been studied in [6,15,18].

1. Union of two cones

A common feature of 5D $\mathcal{N} = 1$ SCFTs is that their Higgs branch can be the union of several hyper-Kähler cones. For example, consider $SU(6)_2$ with $N_f = 8$ fundamental flavors and Chern-Simons (CS) level 2. The SCFT Higgs branch is composed of two cones, each associated with a magnetic quiver (Table 7 in [6])

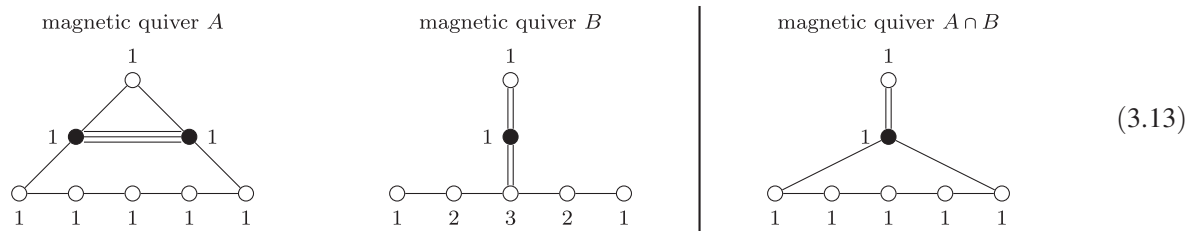


The set of balanced nodes indicates two possible Higgsings: an a_7 and a_1 transition. Since the two cones intersect nontrivially, one should also inspect the magnetic quiver for the intersection between the two cones,



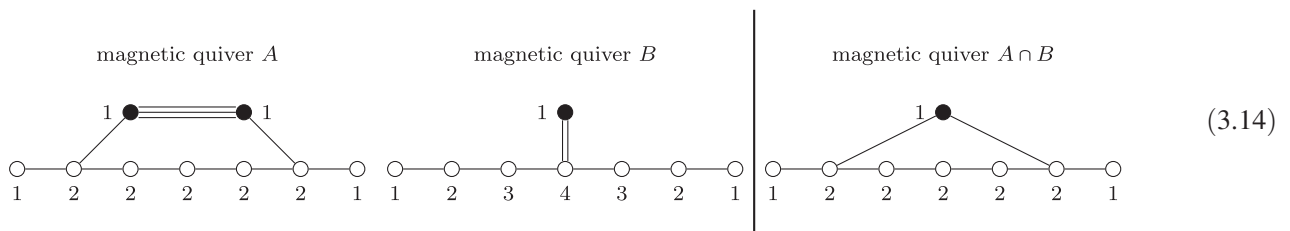
From the intersection quiver, one observes that the a_7 and a_1 transitions are indeed common to both quivers. This means that the a_7 and $a_1 \cong A_1$ transition are part of the intersection of the two cones.

Performing the a_7 Higgsing via the decay algorithm results in



and the 5D $\mathcal{N} = 1$ SCFT whose Higgs branch is given by this set of magnetic quivers is $SU(5)_2$ with $N_f = 6$ fundamental hypermultiplets, see Table 7 in [6].

Alternatively, the a_1 transition leads to



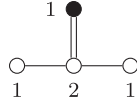
which corresponds to the conformal fixed point of 5D $\mathcal{N} = 1$ $SU(5)_{\frac{5}{2}}$ with $N_f = 7$ fundamental flavors, as follows from comparing the magnetic quivers (Table 2 in [6]). Repeating the decay and fission algorithm reveals the partial Higgsing pattern between 5D SCFTs as depicted in Fig. 16.

In addition to the transitions that are at the intersection of both cones, there exists, in general, a transition \mathfrak{g} that is allowed in one of the magnetic quivers, but not in the other. This is observed in the upper part of Fig. 16 both at $SU(3)_{\frac{3}{2}}, N_f = 3$ and at $SU(3)_2, N_f = 2$. For instance, with $SU(3)_{\frac{3}{2}}, N_f = 3$, the magnetic quivers are the following:

magnetic quiver A



magnetic quiver B



magnetic quiver $A \cap B$



(3.15)

Here, the A_2 transition is only applicable to the left magnetic quiver. Naively, after performing this Higgsing, one of the cones gets Higgsed into a smaller cone, while the other remains the same. We argue against such process. One argument is that the remaining magnetic quiver on the right is not a known magnetic quiver of 5D SCFT, which is fully classified for lower-rank theories.¹⁷ Therefore, what we expect happens is that, once such an asymmetric Higgsing occurs, the cone not involved in the Higgsing disappears entirely. In other words, the hypermultiplets that generate the other cone become free fields.

2. Higgsing between 5D SCFTs

The Higgsings of 5D $\mathcal{N} = 1$ SCFTs is a fairly nontrivial process since the UV theories do not admit a Lagrangian description. Furthermore, massless instantons contribute to the Higgs branch as well, so apart from Higgsings where VEVs are given to hypermultiplets, there are also Higgsings where VEVs are given to the massless instantons. In Fig. 17, we predict via decay and fission a single Higgsing tree where many families of 5D SCFTs, whose magnetic quivers are detailed in [6,15,18], are shown to be Higgsed into each other.

D. 6D $\mathcal{N} = (1,0)$ theories

The existence of 6D supersymmetric theories (e.g., superconformal and little string theories) have revolutionized the understanding of quantum field theories. Again, such theories are inherently strongly coupled and the systematic analysis of the Higgs branch RG flows is

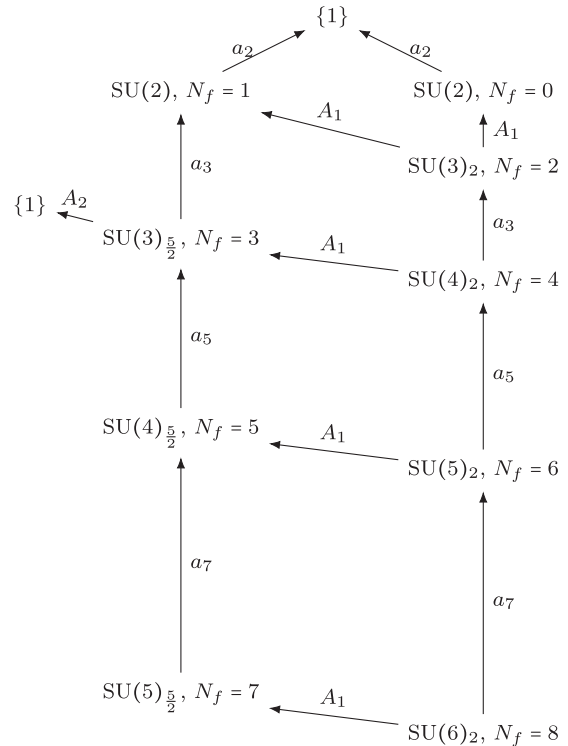


FIG. 16. Higgsing between 5D SCFTs starting from 5D $\mathcal{N} = 1$ $SU(6)_2$ with eight fundamental hypermultiplets. Furthermore, there could be discrete “fat points” in the moduli space as in [82] that are not sensitive in the magnetic quiver and hence the procedure here.

¹⁷An even more concrete example is to take the E_3 theory of $SU(2)$ with two flavors in 5D. This theory’s Higgs branch is a union of two cones that intersect trivially. One of the cones is C_2/\mathbb{Z}_2 , whereas the other is the one- $\mathfrak{su}(3)$ instanton moduli space. If doing the A_1 transition, thus Higgsing away one cone, does not affect the other cone, this means that the remaining 5D SCFT is a rank-1 or rank-0 theory with one- $\mathfrak{su}(3)$ instanton moduli space as its Higgs branch. Such a theory does not exist in the literature and we do not expect it to. This is also observed in the 5-brane web, Higgsing in one direction implies that two maximal decompositions no longer exist. Hence, there are no more two cones.

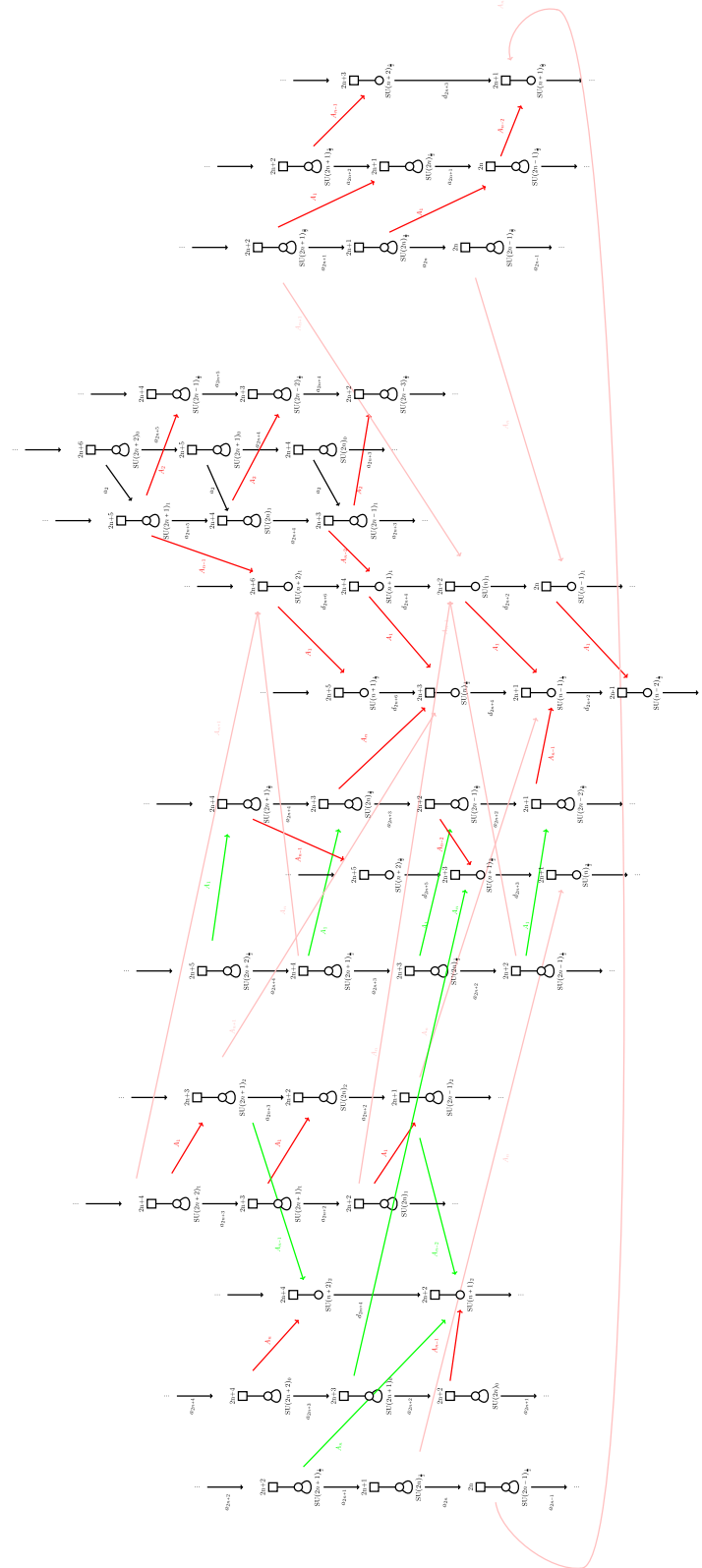


FIG. 17. Pattern of minimal Higgs transitions between 5D $\mathcal{N} = 1$ SCFTs as predicted by the decay and fission algorithm. The 5D gauge theory descriptions are single $SU(N)$ gauge groups, N_f fundamental hypermultiplets (the square box), $N_{\Lambda^2} = 1$ antisymmetric hypermultiplets (the loops), and a CS level. The algorithm utilizes magnetic quivers found in [6,18]. The black transitions are non-Abelian, whereas the pink, green, and red transitions are all Kleinian- $A_k = \mathbb{C}^2/\mathbb{Z}_{k+1}$ type. The reason for using green, red, and pink colored transitions is to improve readability. Despite the drawing, the Higgsing pattern is more apparent when more members of each family are drawn.

challenging, but of utmost importance. Some earlier works include [26,28,30,83–88].

1. $SU(6)$ with $N_f = 14$ fundamentals and one antisymmetric

We consider an example of 6D $\mathcal{N} = (1, 0)$ SCFTs,

$$[\text{Sp}(1)] \overset{\mathfrak{su}(6)}{1} [\text{SU}(14)], \tag{3.16}$$

with a deformation to $SU(6)$ gauge theory with $N_f = 14$ fundamentals and one antisymmetric. For this theory, there is a known superconformal fixed point at the origin of the tensor branch and the magnetic quiver is given by [7,89]

$$\begin{array}{ccccccc} & & & & & \circ & 6 \\ & & & & & | & \\ \circ & - & \circ & \cdots & - & \circ & - & \circ & - & \circ & - & \circ \\ 1 & & 2 & & & 11 & & 12 & & 7 & & 3 \end{array} \tag{3.17}$$

Applying the decay and fission algorithm leads to the Higgsing pattern between 6D $\mathcal{N} = (1, 0)$ SCFTs depicted in Fig. 18. This diagram neatly ties together two features: First, the partial Higgsing pattern of the two families 6D SCFTs defined on a single -1 curve (Fig. 5 in [90]), which have known magnetic quivers. Second, the geometric data reproduce the conjectured Hasse diagram of Fig. 18 in [5].

2. Orbi-instanton and higher-rank E-string theory

Consider the 6D $\mathcal{N} = (1, 0)$ theories originating from M5-branes on an A-type asymptotically locally Euclidean (ALE) space near an M9 plane. Specifically, consider 4 M5-branes, the C^2/\mathbb{Z}_3 ALE space, and choose the trivial

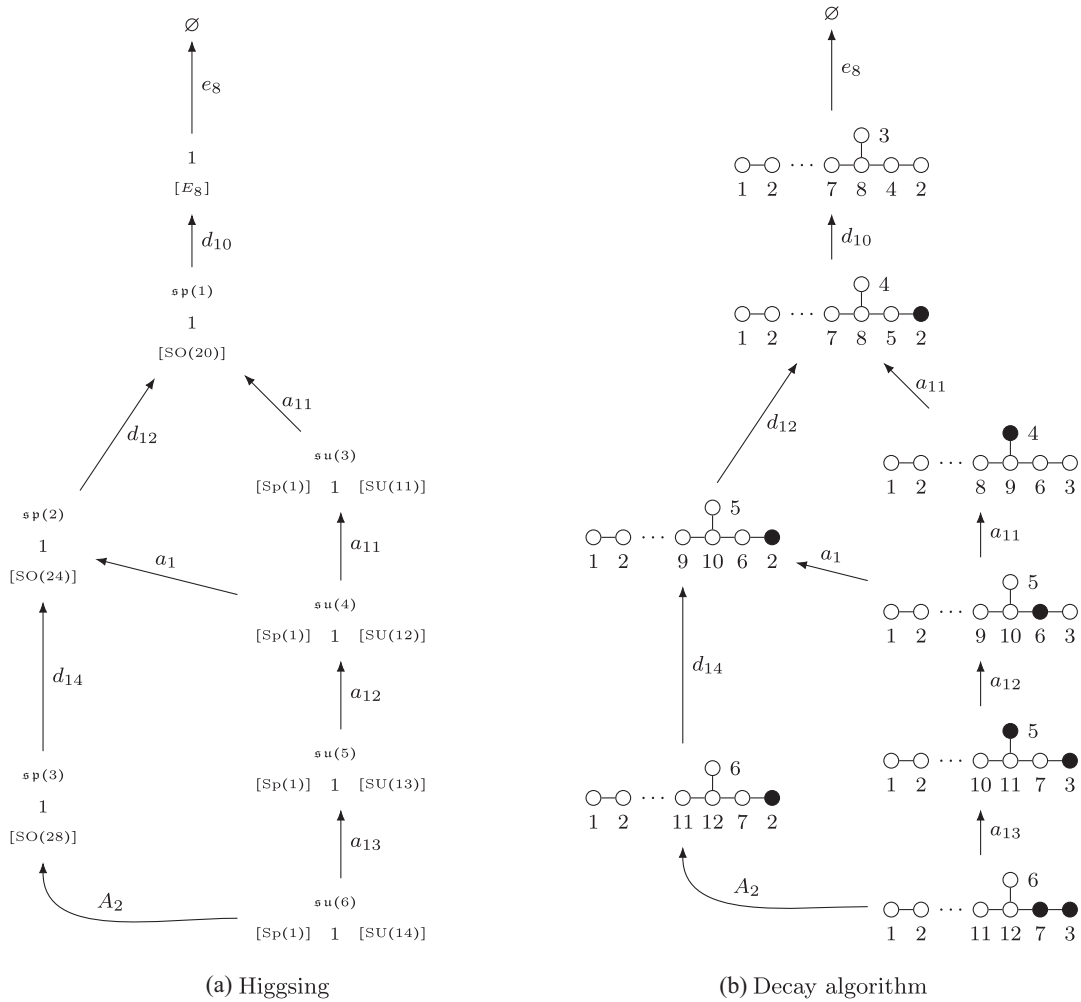


FIG. 18. The Higgsing pattern between 6D SCFTs starting from $SU(6)$ with 14 fundamental hypermultiplets and one antisymmetric hypermultiplet. (a) The SCFTs are labeled by their 6D generalized quiver description $\overset{\mathfrak{g}}{n}_{[G_f]}$, with gauge algebra \mathfrak{g} and flavor symmetry G_f . For example, the theory $\overset{1}{[E_8]}$, i.e., the E-string theory, gives rise to the one- E_8 instanton moduli space in the tensionless limit. (b) The Higgsing pattern derived via the decay algorithm (no fission occurs here).

embedding $\mathbb{Z}_3 \hookrightarrow E_8$,

$$\begin{aligned}
 & [\text{SU}(3)] \begin{array}{c} \mathfrak{su}(3) \\ 2 \\ [N_f=1] \end{array} - \begin{array}{c} \mathfrak{su}(2) \\ 2 \\ [E_8] \end{array} - \begin{array}{c} \mathfrak{su}(1) \\ 2 \\ [E_8] \end{array} - 1 \\
 & \cong \begin{array}{c} \mathfrak{su}(3) \\ 2 \\ [\text{SU}(4)] \end{array} - \begin{array}{c} \mathfrak{su}(2) \\ 2 \\ [E_8] \end{array} - \begin{array}{c} \mathfrak{su}(1) \\ 2 \\ [E_8] \end{array} - 1, \quad (3.18)
 \end{aligned}$$

wherein the last description keeps the flavor symmetries manifest. The magnetic quiver is readily available [7,89] and serves as starting point for the decay and fission algorithm. The result is the Higgsing pattern of Fig. 19, which can be translated to the Higgs mechanism of the 6D theory shown in Fig. 20.

A few comments are in order. First, the 6D theory

$$\begin{array}{c} \mathfrak{su}(1) \\ 2 \\ [\text{SU}(3)] \end{array} - \begin{array}{c} \mathfrak{su}(2) \\ 2 \\ [E_8] \end{array} - \begin{array}{c} \mathfrak{su}(1) \\ 2 \\ [E_8] \end{array} - 1 \quad (3.19)$$

admits an RG flow to the rank-4 E-string theory

$$2 - 2 - 2 - 2 - \frac{1}{[E_8]}, \quad (3.20)$$

i.e., four M5-branes near an M9 plane. The transition type is deduced as follows:

which is, in fact, the twisted affine a_2 Dynkin quiver.

Next, in Fig. 20 there are two 6D theories with a G_2 global symmetry factor that can flow to the rank-2 E-string theory. To begin with, consider

$$\begin{array}{c} \mathfrak{su}(2) \\ 2 \\ [G_2] \end{array} - \begin{array}{c} \mathfrak{su}(1) \\ 2 \\ [E_8] \end{array} - 1 \quad (3.22)$$

and the g_2 Higgs branch flow is deduced via

which produced the affine G_2 Dynkin diagram due to $\text{gcd} = 3$ of the decay product. The other 6D theory is

$$\begin{array}{c} \mathfrak{su}(1) \\ 2 \\ [G_2] \end{array} - \begin{array}{c} \mathfrak{su}(2) \\ 2 \\ [E_7] \end{array} - 1 \quad (3.24)$$

and the transverse geometry of the RG flow is seen via

which again results in the affine G_2 Dynkin quiver.

Via similar arguments, one deduces that the transition geometries for the RG flows

$$\begin{array}{c} \mathfrak{su}(1) \\ 2 \\ [\text{SO}(7)] \end{array} - \begin{array}{c} \mathfrak{sp}(1) \\ 1 \\ [\text{SO}(16)] \end{array} \xrightarrow{b_9} 2 - \frac{1}{[E_8]} \quad (3.26)$$

$$\begin{array}{c} \mathfrak{su}(2) \\ 2 \\ [\text{SO}(7)] \end{array} - \frac{1}{[E_7]} \xrightarrow{b_3} 2 - \frac{1}{[E_8]} \quad (3.27)$$

ending in the rank-2 E-string theory.

In addition to the decays there are also fissions. A natural fission occurs for the orbi-instanton theory of N M5-branes on $\mathbb{C}^2/\mathbb{Z}_k$ with trivial homomorphism $[1^k]: \mathbb{Z}_k \hookrightarrow E_8$ (assuming $N - 1 \geq k$),

$$\begin{aligned}
 & \overbrace{\begin{array}{c} \mathfrak{su}(k) \quad \mathfrak{su}(k) \quad \dots \quad \mathfrak{su}(k) \quad \mathfrak{su}(k) \quad \mathfrak{su}(k-1) \quad \dots \quad \mathfrak{su}(2) \quad \mathfrak{su}(1) \\ 2 \quad 2 \quad \dots \quad 2 \quad 2 \quad 2 \quad \dots \quad 2 \quad 2 \quad 2 \quad 2 \\ [\text{SU}(k)] \quad [N_f=1] \quad [E_8] \end{array}}^{N-1 \text{ curves of self-intersection}-2} \\
 & \longrightarrow \overbrace{\begin{array}{c} \mathfrak{su}(k) \quad \dots \quad \mathfrak{su}(k) \quad \mathfrak{su}(k-1) \quad \dots \quad \mathfrak{su}(2) \quad \mathfrak{su}(1) \\ 2 \quad 2 \quad \dots \quad 2 \quad 2 \quad \dots \quad 2 \quad 2 \\ [\text{SU}(k)] \quad [N_f=1] \quad [E_8] \quad [E_8] \end{array}}^{N-2 \text{ curves of self-intersection}-2} \sqcup 1 \quad (3.28)
 \end{aligned}$$

into the orbi-instanton theory with $N - 1$ M5-branes and a single E-string theory, provided $N - 2 \geq k$. In the limiting case $N - 1 = k$, no fission occurs, as removing an M5 renders it impossible to realize the trivial boundary conditions $[1^k]$ in a supersymmetry preserving way. That is the reason why the initial theory (3.18) cannot fission, while its daughter theory

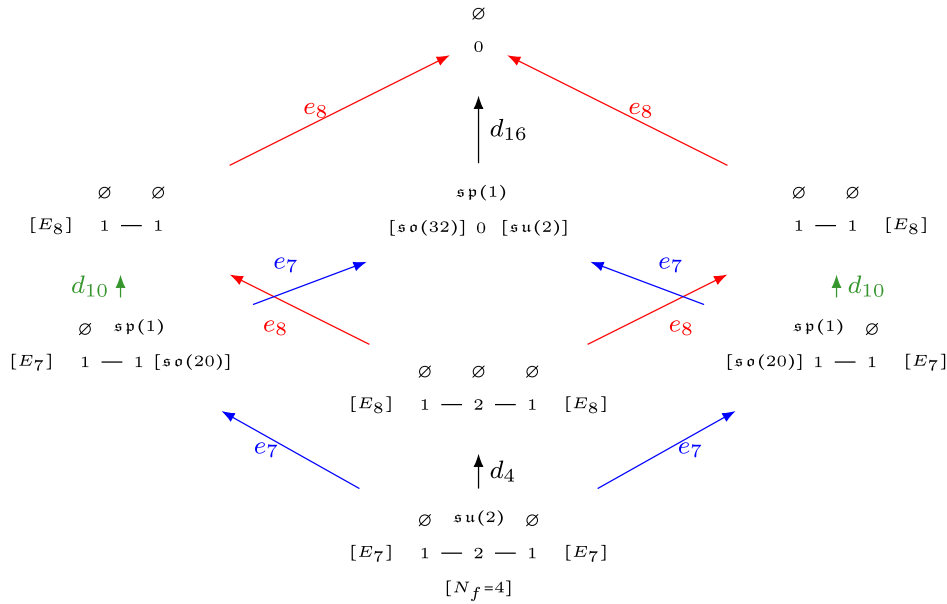


FIG. 22. Higgsing pattern of LST (3.31).

$$\begin{array}{ccc}
 \emptyset & \text{su}(2) & \emptyset \\
 [E_7] & 1 - 2 - 1 & [E_7] \\
 & [N_f=4] &
 \end{array} \tag{3.31}$$

and already provides an intricate pattern of Higgs branch RG flows predicted by the decay and fission algorithm. The starting point is the magnetic quiver [33]

$$\tag{3.32}$$

for which the decay process traces out the Hasse diagram shown in Fig. 21.

Here, a new phenomenon appears: the magnetic quiver after the d_4 transitions is reducible, see Sec. II B. Therefore, deriving the geometry of the slice requires a rebalancing node for each irreducible component. In detail,

$$\tag{3.33}$$

so that the transition is identified as d_4 . The reducibility can be understood from the physical system: one starts from (3.31) and ends with a curve configuration that does not support any gauge algebras. The M-theory picture is that of two M9 walls on a finite interval with one M5-brane inside each E_8 wall. Each of them yields an affine E_8 Dynkin quiver for its magnetic degrees of freedom (i.e., Higgs branch moduli).

The magnetic quivers in Fig. 21 can be identified with descendants of the little string theory (3.31) and the predicted Higgs branch RG-flow pattern is summarized in Fig. 22.

Note that the initial LST curve configuration $1 - 2 - 1$ can reach the LST defined on a curve 0 of vanishing self-intersection by collapsing each of the initial -1 curves. The Higgs branch RG flows of these 0 curve models have been analyzed in [35].

A *second example*. A more elaborate example is given by the choice of $([1^2], [1^2])$ embeddings [92]

$$\begin{array}{ccccccc}
 & \emptyset & \text{su}(1) & \text{su}(2) & \text{su}(1) & \emptyset & \\
 [E_8] & 1 & \text{---} & 2 & \text{---} & 2 & \text{---} & 2 & \text{---} & 1 & [E_8] \\
 & & & & & [N_f=2] & & & & &
 \end{array} \tag{3.34}$$

which preserves the full $E_8 \times E_8$ symmetry. Starting again from the magnetic quiver [33]

$$\tag{3.35}$$

one can apply the decay and fission algorithm to trace out the Hasse diagram, shown in Fig. 23.

This already contains some more new features that deserve to be commented on. First, the bottom a_3 transition again leads to a reducible quiver

$$\tag{3.36}$$

and the geometry of the slice is deduced again by a rebalancing node for each reducible component. In addition, each reducible component has $\text{gcd} = 2$, such that non-simply-laced edges are required. As a result, the slice is read off to be a_3 . Physically, this transition takes the curve configuration (3.34) with nontrivial gauge algebras to the same curve configuration, but with trivial gauge algebras. The reason why this yields two reducible magnetic quivers

is understood from the M-theory picture: two M9 walls on a finite interval with two M5-branes inside each M9. This setting also illuminates the subsequent diamond of A_1 fissions: each stack of two M5s can fission independently. The M5 that is moved off along the, here right-hand side, M9 leads to the LST $1 - 1[E_8]$.

Similarly, the b_3 transition in Fig. 23 is the result of a reducible quiver after a decay transition,

$$\tag{3.37}$$

such that the slice is read off by introducing two rebalancing nodes. Here, the two irreducible quivers have $\text{gcd} = 2$ and 1, respectively. The geometry is identified as b_3 . Again, the transition starts from the curve configuration $1 - 2 - 2 - 1$ with nontrivial gauge algebras and ends up with trivial gauge algebras. Thus, the reducible magnetic quiver is clear from the M-theory picture: one M9 wall hosts two M5-branes, while the other holds only one. As a result, there exists a subsequent A_1 fission of the stack of two M5s.

Likewise, the b_9 transition in Fig. 23 stems from a nontrivial gcd of the decay product,

$$\tag{3.38}$$

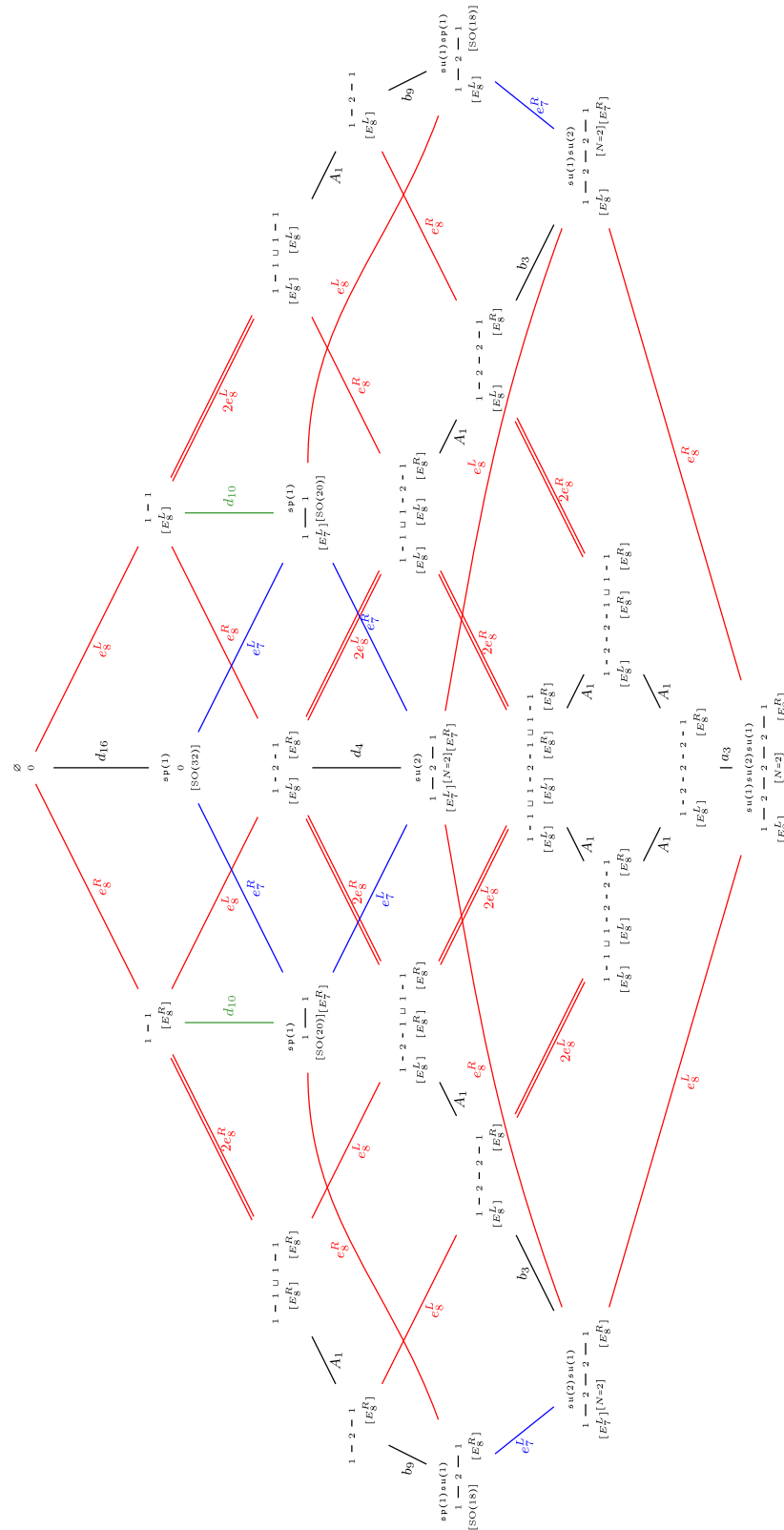


FIG. 23. Exemplary Hasse diagram for the LST (3.34). In addition to decays, there are fissions present. These originate from the fact that the system has M-theory description of two M9 walls at the ends of the interval S^1/\mathbb{Z}_2 with two M5-branes on each wall. Then, the stacks of M5 can undergo fission. Note also that the Hasse diagram of Fig. 21 is clearly contained as a subdiagram.

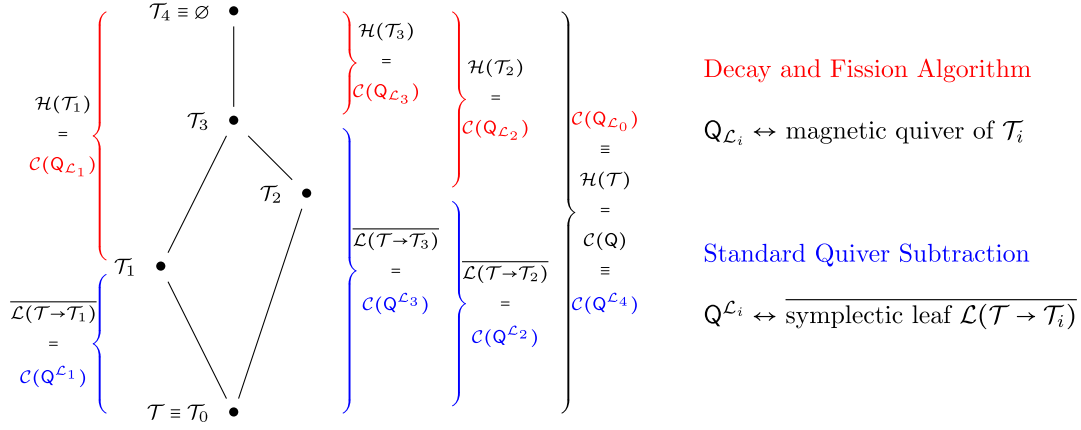


FIG. 24. Higgs branch Hasse diagram of a theory \mathcal{T} with eight supercharges in $d = 3, 4, 5, 6$. A theory with this Higgsing pattern is, for example, the 6D $\mathcal{N} = (1, 0)$ $SU(4)$ theory with $N_f = 12$ and $N_{\Lambda^2} = 1$, see Figs. 6–9 in [5]. Both decay and fission, as well as quiver subtraction, produce magnetic quivers that capture certain transverse slices. Denote $X = \mathcal{H}(\mathcal{T}) = \mathcal{C}(\mathcal{Q})$ the entire symplectic singularity. Also, label the leaves \mathcal{L}_i with the theories \mathcal{T}_i at the end of the Higgs branch RG flow: i.e., $\mathcal{L}_i \equiv \mathcal{L}(\mathcal{T} \rightarrow \mathcal{T}_i)$. Then the slice $\mathcal{S}(\mathcal{L}_i, X) = \mathcal{H}(\mathcal{T}_i)$ is the Higgs branch of the Higgsed theory \mathcal{T}_i and equals the Coulomb branch $\mathcal{C}(\mathcal{Q}_{\mathcal{L}_i})$ of the quiver $\mathcal{Q}_{\mathcal{L}_i}$. These are results obtained from the decay and fission algorithm, introduced in this work. In contrast, the slices $\mathcal{S}(\mathcal{L}_0, \mathcal{L}_i) = \tilde{\mathcal{L}}_i = \mathcal{C}(\mathcal{Q}^{\mathcal{L}_i})$ are described by the quivers $\mathcal{Q}^{\mathcal{L}_i}$ obtained from the standard quiver subtraction.

such that the magnetic quiver for the slice has a non-simply-laced edge. As with the other two examples, the starting point is a $1 - 2 - 1$ curve configuration with gauge algebras that become trivial during the decay. The decay product originates from the M-theory setting of two M9 walls on a finite interval and one wall contains a stack of two M5-branes. Again, this opens up the possibility of a subsequent fission into $1 - 1[E_8] \sqcup 1 - 1[E_8]$, i.e., two LSTs.

IV. DISCUSSION, CONCLUSIONS, AND OPEN QUESTIONS

Magnetic quivers have proven to be immensely useful for both providing insights in Higgs branches of strongly coupled supersymmetric theories and revealing geometric features. Particularly important are algorithms of quiver operations. In this work, we introduced the decay and fission algorithm, which at its core only relies on linear algebra. Beyond the simplicity, this algorithm allows us to determine precisely the phase diagram of the theory with the Higgs branch of the Higgsed theories identified along with the transverse slices that underline the geometric structure of the vacuum. The former allowed us to find the Higgsing diagram of SCFTs and gauge theories with eight supercharges in dimensions 3–6 of which a plethora of examples are shown in the text.

A. Comparison with standard quiver subtraction

We now see how the decay and fission algorithm distinguishes from another similar but fundamentally different quiver operation: quiver subtraction [5]. It is insightful to compare the two methods and analyze the different quivers that arise. It is insightful to compare the

two methods and analyze the different quivers that arise, see Fig. 24. In several examples, both techniques have been applied and presented: e.g., Figs. 5 and 8–11. An immediate observation is that the decay and fission algorithm keeps the shape of the quiver similar after subtraction, whereas quiver subtraction drastically changes the shape due to rebalancing gauge nodes. Here, the aim is to discuss the geometric meaning behind the two different sets of magnetic quivers.

Upon Higgsing a theory \mathcal{T} to a theory \mathcal{T}' , the Higgs branch geometry changes: a coarse signature of this change is the fact that $\dim \mathcal{H}(\mathcal{T}') < \dim \mathcal{H}(\mathcal{T})$. A finer relation is the fact that $\mathcal{H}(\mathcal{T})$ is a conical symplectic singularity with a (finite) stratification into symplectic leaves, and $\mathcal{H}(\mathcal{T}')$ appears as a transverse slice in $\mathcal{H}(\mathcal{T})$ to a certain leaf. Because of these restrictions, it is often possible to turn the logic around and to identify, for each transverse slice in $\mathcal{H}(\mathcal{T})$, which theory \mathcal{T}' possesses this slice as its Higgs branch. Therefore, understanding the geometry of transverse slices in $\mathcal{H}(\mathcal{T})$ is often sufficient to identify the possible Higgsings of a given theory \mathcal{T} .

The decay and fission algorithm introduced in this work achieves precisely this goal, in cases where $\mathcal{H}(\mathcal{T})$ admits a “unitary magnetic quiver,” i.e., when there is a quiver \mathcal{Q} with unitary gauge nodes such that $\mathcal{C}^{3D\mathcal{N}=4}(\mathcal{Q}) = \mathcal{H}(\mathcal{T})$. Specifically, the decay and fission algorithm produces

- (i) the poset of symplectic leaves and elementary degenerations between adjacent leaves; and
- (ii) for each leaf \mathcal{L} in $\mathcal{H}(\mathcal{T})$ a magnetic quiver $\mathcal{Q}_{\mathcal{L}}(\mathcal{T})$ for the transverse slice to this leaf.

It is then often possible to identify, using techniques developed elsewhere, theories $\mathcal{T}_{\mathcal{L}}$ with Higgs branch admitting magnetic quivers $\mathcal{Q}_{\mathcal{L}}(\mathcal{T})$. Combined with output

(i), this then produces the complete Higgsing graph for \mathcal{T} . Multiple examples have been detailed in Sec. III. Note that a primitive version of the decay and fission algorithm was applied to height 2 nilpotent orbits in [40]. There are also quiver algorithms that achieve this to some level of success in [26,30,65].

Before this, it is important to mention that (i) can also be obtained from the previously introduced quiver subtraction algorithm [5], which produces

- (i) the poset of symplectic leaves and elementary degenerations between adjacent leaves; and
- (ii') for each leaf \mathcal{L} in $\mathcal{H}(\mathcal{T})$ a magnetic quiver $\mathbf{Q}^{\mathcal{L}}(\mathcal{T})$ for the closure of this leaf.

Here the poset is obtained inductively beginning from the higher-dimensional leaves.

We note that both algorithms output the poset (i): this should be seen as an internal consistency check of the validity of the whole procedure. But the magnetic quivers are definitely not the same and reflect distinct physical phenomena, see Figs. 5 and 8–11. In terms of Higgsing \mathcal{T} , this means that the quiver subtraction algorithm can at best provide the Higgs branch dimension of \mathcal{T}' which is unlikely to be enough information to determine the theory \mathcal{T}' . On the other hand, the decay and fission tells everything about the Higgs branch of \mathcal{T}' , a substantial amount of information that allows an easy identification of \mathcal{T}' .

Finally, the two algorithms are conceptually different: while quiver subtraction is an iterative process relying in an input list of minimal degenerations, in contrast, decay and fission is “holistic” in nature. More concretely, the latter takes the magnetic quiver and outputs the entire Hasse diagram solely from the shape of the quiver data (A, K) , see Sec. II C. The appearing minimal degenerations are then by-products of the first step. For instance, more complicated quivers such as non-simply-laced quivers with lengths greater than 2 or with gauged groups having more than one adjoint hypermultiplet, the list of minimal degenerations is likely incomplete. This makes it challenging for the quiver subtraction algorithm, but the decay and fission algorithm, which only relies on the balance of the gauge groups and their relative position in the quiver, generates the phase diagram without difficulty.

The standard quiver subtraction algorithm [5] had undergone several improvements [17,29,52] to handle quivers with more unique features (such as gauge nodes with adjoint hypermultiplets, non-simply-laced edges, and stacks of affine Dynkin quivers). The decay and fission algorithm now incorporates all these features as well. However, in the future, it is possible that both algorithms will require further refinements as we explore the quiver landscape further; see below for open questions.

B. Further applications and future directions

The decay and fission algorithm has other interesting applications beyond just Higgsing theories.

1. Identifying any transverse slice

The standard quiver subtraction introduced in [5] and the decay and fission algorithm, introduced in this paper, can be combined to generate 3D $\mathcal{N} = 4$ quivers whose Coulomb branch describes any transverse slices between two symplectic leaves in a Hasse diagram. This is clear since combining (ii) in decay and fission and (ii') in quiver subtraction allows one to obtain magnetic quivers $\mathbf{Q}_{\mathcal{L}}^{\mathcal{L}'}$ for the transverse slice to \mathcal{L} into $\overline{\mathcal{L}'}$ for any $\mathcal{L} < \mathcal{L}'$.

However, before enthusiastically using this method to find quivers whose Coulomb branch corresponds to more exotic slices such as the one-dimensional non-normal slice denoted as m , it is important to note that the procedure *may not* apply to quivers with decorations. These appear during standard subtraction on quivers containing multiple affine Dynkin diagrams or quivers containing gauge nodes with adjoint hypermultiplets [52]. We leave such possibilities for the future when decorated quivers are better understood.

A final remark concerns appearing product theories after fissions. Recalling the introductory cartoon in Fig. 1 and its detailed version in Fig. 5, one observes leaves with product theories, but the Hasse diagram does not contain the product of the Hasse diagram as subgraph. This is a manifestation of the known fact (Fig. 3 in [29]) that the Hasse diagram of a transverse slice does not have to be a subdiagram of the Hasse diagram of the full theory.

2. Identifying elementary slices

Classifying all elementary slices (to be precise, these are isolated symplectic singularities [50,93]) has long been an intriguing goal in the mathematics community. Recently [29,60], many new quivers that correspond to elementary slices have been discovered and added to the dictionary. An interesting application of the decay and fission algorithm is that it can assist in this search, as explained in Sec. II E. An obvious extension of the results obtained in that section, in which we restricted ourselves to quivers with three nodes or less, is the classification of isolated singularities corresponding to unitary quivers with arbitrarily many nodes.

3. Finding new SCFTs

The classification of SCFTs with eight supercharges in various dimensions has long been an interesting goal of the community. The decay and fission algorithm acting as a Higgsing algorithm can help find missing SCFTs. If, for example, a complete classification up to rank- r 4D $\mathcal{N} = 2$ SCFT is made, then given a rank- r SCFT \mathcal{T} , all the theories \mathcal{T}' it can Higgs to as indicated by our algorithm *must* appear in the classification as well.

4. Orthosymplectic quivers

The decay and fission algorithm applies to a large, but still restricted set of (magnetic) quivers. Given the wealth of known magnetic quivers, the decay and fission algorithm

needs to be extended to accommodate further quiver theories, for instance, orthosymplectic quivers. For those theories, even standard quiver subtraction is still under development.

Moreover, for all examples considered here, the practical implementation (1)–(3) is equivalent to the decay algorithm, provided no fission can appear. It might, however, be that some new minimal transitions are found. These would not be covered by (1)–(3), but the decay and fission algorithm is fully capable to detect them. This is because the decay and fission algorithm *does not* rely on a list of known minimal transition (which is necessarily incomplete).

In the case of orthosymplectic quivers, one thing that prevents us from constructing the standard quiver subtraction is that we do not know all orthosymplectic quivers that correspond to minimal transitions. The number of inequivalent orthosymplectic quivers that leads to the same moduli space seems more diverse than unitary quivers (see, e.g., orthosymplectic quivers of one- E_6 instanton moduli space in [10,12,51]). On the other hand, the decay and fission algorithm, as mentioned above, does not require obtaining a list of minimal transitions. So finding all possible daughter/granddaughter orthosymplectic quivers that it can decay to should be a much simpler task.

5. Higgs branch RG flows

One application of Higgs branch RG flows between SCFTs already seen in the literature is to prove certain maximization theorems, for instance, the “a theorem” that a anomaly decreases under RG flows in 6D SCFTs in [36], the “c theorem” for c anomaly in [84], and also other quantities such as the F theorem for 5D $\mathcal{N} = 1$ SCFTs that the free energy decreases under Higgs branch RG flows in [94]. With the decay and fission algorithm, we now have all possible minimal Higgsings for these SCFTs, which can

be easily missed in the literature and can give a more complete proof of these theorems.

ACKNOWLEDGMENTS

We thank Christopher Beem, Simone Giacomelli, Julius Grimminger, Jie Gu, Amihay Hanany, Patrick Jefferson, Yunfeng Jiang, Monica Kang, Hee-Cheol Kim, Sung-Soo Kim, Craig Lawrie, Lorenzo Mansi, Carlos Nunez, Matteo Sacchi, and Sakura Schäfer-Nameki for many discussions on this topic. We are grateful for support and stimulating discussions during the following events: A. B. at String Theory Seminar of DESY/University Hamburg on June 26, 2023. M. S. at workshop “Symplectic Singularities and Supersymmetric QFT” in Amiens on July 20, 2023. Z. Z. at Oxford’s String Theory seminar on January 22, 2023, KIAS String Seminars on February 13, 2023, Swansea University on May 31, 2023, Seoul National University CTP seminars October 17, 2023, and IPMU string-math seminar on December 22, 2023. A. B. is partly supported by the ERC Consolidator Grant No. 772408-Stringlandscape. This research was supported in part by Grant No. NSF PHY-2309135 to the Kavli Institute for Theoretical Physics (KITP). M. S. is supported by Austrian Science Fund (FWF) [grant DOI: 10.55776/STA73], START project “Phases of quantum field theories: Symmetries and vacua” STA 73-N. M. S. also acknowledges support from the Faculty of Physics, University of Vienna. M. S. was previously supported by Shing-Tung Yau Center, Southeast University. Z. Z. is supported by the ERC Consolidator Grant No. 864828 “Algebraic Foundations of Supersymmetric Quantum Field Theory” (SCFTAlg). Z. Z. is grateful of the hospitality of New College, Oxford where the final stages of this work is completed.

-
- [1] F. Englert and R. Brout, Broken symmetry and the mass of gauge vector mesons, *Phys. Rev. Lett.* **13**, 321 (1964).
 - [2] P. W. Higgs, Broken symmetries and the masses of gauge bosons, *Phys. Rev. Lett.* **13**, 508 (1964).
 - [3] G. S. Guralnik, C. R. Hagen, and T. W. B. Kibble, Global conservation laws and massless particles, *Phys. Rev. Lett.* **13**, 585 (1964).
 - [4] T. W. B. Kibble, Symmetry breaking in non-Abelian gauge theories, *Phys. Rev.* **155**, 1554 (1967).
 - [5] A. Bourget, S. Cabrera, J. F. Grimminger, A. Hanany, M. Sperling, A. Zajac, and Z. Zhong, The Higgs mechanism—Hasse diagrams for symplectic singularities, *J. High Energy Phys.* **01** (2020) 157.
 - [6] S. Cabrera, A. Hanany, and F. Yagi, Tropical geometry and five dimensional Higgs branches at infinite coupling, *J. High Energy Phys.* **01** (2019) 068.
 - [7] S. Cabrera, A. Hanany, and M. Sperling, Magnetic quivers, Higgs branches, and 6d $N = (1, 0)$ theories, *J. High Energy Phys.* **06** (2019) 071.
 - [8] A. Bourget, S. Cabrera, J. F. Grimminger, A. Hanany, and Z. Zhong, Brane webs and magnetic quivers for SQCD, *J. High Energy Phys.* **03** (2020) 176.
 - [9] S. Cabrera, A. Hanany, and M. Sperling, Magnetic quivers, Higgs branches, and 6d $N = (1, 0)$ theories—orthogonal and symplectic gauge groups, *J. High Energy Phys.* **02** (2020) 184.

- [10] A. Bourget, J. F. Grimminger, A. Hanany, M. Sperling, and Z. Zhong, Magnetic quivers from brane webs with O5 planes, *J. High Energy Phys.* **07** (2020) 204.
- [11] A. Bourget, J. F. Grimminger, A. Hanany, M. Sperling, G. Zafrir, and Z. Zhong, Magnetic quivers for rank 1 theories, *J. High Energy Phys.* **09** (2020) 189.
- [12] A. Bourget, J. F. Grimminger, A. Hanany, R. Kalveks, M. Sperling, and Z. Zhong, Magnetic lattices for orthosymplectic quivers, *J. High Energy Phys.* **12** (2020) 092.
- [13] C. Closset, S. Schafer-Nameki, and Y.-N. Wang, Coulomb and Higgs branches from canonical singularities: Part 0, *J. High Energy Phys.* **02** (2021) 003.
- [14] M. Aghvami, F. Carta, S. Dwivedi, H. Hayashi, S.-S. Kim, and F. Yagi, Five-brane webs, Higgs branches and unitary/orthosymplectic magnetic quivers, *J. High Energy Phys.* **12** (2020) 164.
- [15] M. van Beest, A. Bourget, J. Eckhard, and S. Schafer-Nameki, (Symplectic) leaves and (5d Higgs) branches in the poly(go)nesian tropical rain forest, *J. High Energy Phys.* **11** (2020) 124.
- [16] S. Giacomelli, M. Martone, Y. Tachikawa, and G. Zafrir, More on $\mathcal{N} = 2$ S-folds, *J. High Energy Phys.* **01** (2021) 054.
- [17] A. Bourget, S. Giacomelli, J. F. Grimminger, A. Hanany, M. Sperling, and Z. Zhong, S-fold magnetic quivers, *J. High Energy Phys.* **02** (2021) 054.
- [18] M. Van Beest, A. Bourget, J. Eckhard, and S. Schäfer-Nameki, (5d RG-flow) trees in the tropical rain forest, *J. High Energy Phys.* **03** (2021) 241.
- [19] C. Closset, S. Giacomelli, S. Schafer-Nameki, and Y.-N. Wang, 5d and 4d SCFTs: Canonical singularities, trinions and S-dualities, *J. High Energy Phys.* **05** (2021) 274.
- [20] M. Aghvami, F. Carta, S. Dwivedi, H. Hayashi, S.-S. Kim, and F. Yagi, Factorised 3d $\mathcal{N} = 4$ orthosymplectic quivers, *J. High Energy Phys.* **05** (2021) 269.
- [21] A. Bourget, J. F. Grimminger, M. Martone, and G. Zafrir, Magnetic quivers for rank 2 theories, *J. High Energy Phys.* **03** (2022) 208.
- [22] M. van Beest and S. Giacomelli, Connecting 5d Higgs branches via Fayet-Iliopoulos deformations, *J. High Energy Phys.* **12** (2021) 202.
- [23] M. Sperling and Z. Zhong, Balanced B and D-type orthosymplectic quivers—Magnetic quivers for product theories, *J. High Energy Phys.* **04** (2022) 145.
- [24] S. Nawata, M. Sperling, H. E. Wang, and Z. Zhong, Magnetic quivers and line defects—On a duality between 3d $\mathcal{N} = 4$ unitary and orthosymplectic quivers, *J. High Energy Phys.* **02** (2022) 174.
- [25] M. Aghvami, F. Carta, S. Dwivedi, H. Hayashi, S.-S. Kim, and F. Yagi, Exploring the orthosymplectic zoo, *J. High Energy Phys.* **05** (2022) 054.
- [26] S. Giacomelli, M. Moleti, and R. Savelli, Probing 7-branes on orbifolds, *J. High Energy Phys.* **08** (2022) 163.
- [27] A. Hanany and M. Sperling, Magnetic quivers and negatively charged branes, *J. High Energy Phys.* **11** (2022) 010.
- [28] M. Fazzi and S. Giri, Hierarchy of RG flows in 6d (1, 0) orbi-instantons, *J. High Energy Phys.* **12** (2022) 076.
- [29] A. Bourget and J. F. Grimminger, Fibrations and Hasse diagrams for 6d SCFTs, *J. High Energy Phys.* **12** (2022) 159.
- [30] M. Fazzi, S. Giacomelli, and S. Giri, Hierarchies of RG flows in 6d (1, 0) massive E-strings, *J. High Energy Phys.* **03** (2023) 089.
- [31] S. Nawata, M. Sperling, H. E. Wang, and Z. Zhong, 3d $\mathcal{N} = 4$ mirror symmetry with 1-form symmetry, *SciPost Phys.* **15**, 033 (2023).
- [32] A. Bourget, J. F. Grimminger, A. Hanany, R. Kalveks, M. Sperling, and Z. Zhong, A tale of N cones, *J. High Energy Phys.* **09** (2023) 073.
- [33] M. Del Zotto, M. Fazzi, and S. Giri, The Higgs branch of heterotic ALE instantons, *J. High Energy Phys.* **01** (2024) 167.
- [34] C. Lawrie and L. Mansi, The Higgs branch of heterotic LSTs: Hasse diagrams and generalized symmetries, [arXiv:2312.05306](https://arxiv.org/abs/2312.05306).
- [35] L. Mansi and M. Sperling, Unravelling T-duality: Magnetic quivers in rank-zero little string theories, [arXiv:2312.12510](https://arxiv.org/abs/2312.12510).
- [36] M. Fazzi, S. Giri, and P. Levy, Proving the 6d a-theorem with the double affine Grassmannian, [arXiv:2312.17178](https://arxiv.org/abs/2312.17178).
- [37] G. Ferlito and A. Hanany, A tale of two cones: The Higgs branch of $\text{Sp}(n)$ theories with $2n$ flavours, [arXiv:1609.06724](https://arxiv.org/abs/1609.06724).
- [38] S. Cremonesi, A. Hanany, and A. Zaffaroni, Monopole operators and Hilbert series of Coulomb branches of 3d $\mathcal{N} = 4$ gauge theories, *J. High Energy Phys.* **01** (2014) 005.
- [39] S. Cremonesi, G. Ferlito, A. Hanany, and N. Mekareeya, Coulomb branch and the moduli space of instantons, *J. High Energy Phys.* **12** (2014) 103.
- [40] S. Cabrera and A. Hanany, Quiver subtractions, *J. High Energy Phys.* **09** (2018) 008.
- [41] J. Eckhard, S. Schäfer-Nameki, and Y.-N. Wang, Trifectas for T_N in 5d, *J. High Energy Phys.* **07** (2020) 199.
- [42] M. Martone, Testing our understanding of SCFTs: A catalogue of rank-2 $\mathcal{N} = 2$ theories in four dimensions, *J. High Energy Phys.* **07** (2022) 123.
- [43] C. Closset, S. Schäfer-Nameki, and Y.-N. Wang, Coulomb and Higgs branches from canonical singularities. Part I. Hypersurfaces with smooth Calabi-Yau resolutions, *J. High Energy Phys.* **04** (2022) 061.
- [44] L. Santilli and M. Tierz, Crystal bases and three-dimensional $\mathcal{N} = 4$ Coulomb branches, *J. High Energy Phys.* **03** (2022) 073.
- [45] G. Arias-Tamargo, A. Bourget, and A. Pini, Discrete gauging and Hasse diagrams, *SciPost Phys.* **11**, 026 (2021).
- [46] J. Mu, Y.-N. Wang, and H. N. Zhang, 5d SCFTs from isolated complete intersection singularities, *J. High Energy Phys.* **02** (2024) 155.
- [47] H. Kraft and C. Procesi, Minimal singularities in GL_n , *Inventiones Math.* **62**, 503 (1980).
- [48] H. Kraft and C. Procesi, On the geometry of conjugacy classes in classical groups, *Commentarii mathematici Helvetici* **57**, 539 (1982).

- [49] B. Fu, D. Juteau, P. Levy, and E. Sommers, Generic singularities of nilpotent orbit closures, *Adv. Math.* **305**, 1 (2017).
- [50] G. Bellamy, C. Bonnafé, B. Fu, D. Juteau, P. Levy, and E. Sommers, A new family of isolated symplectic singularities with trivial local fundamental group, *Proc. London Math. Soc.* **126**, 1496 (2023).
- [51] A. Bourget, J. F. Grimminger, A. Hanany, R. Kalveks, M. Sperling, and Z. Zhong, Folding orthosymplectic quivers, *J. High Energy Phys.* **12** (2021) 070.
- [52] A. Bourget, J. F. Grimminger, A. Hanany, and Z. Zhong, The Hasse diagram of the moduli space of instantons, *J. High Energy Phys.* **08** (2022) 283.
- [53] A. Bourget, M. Sperling, and Z. Zhong, Decay and fission of magnetic quivers, *Phys. Rev. Lett.* **132**, 221603.
- [54] O. Chacaltana, J. Distler, and Y. Tachikawa, Nilpotent orbits and codimension-two defects of 6d $N = (2, 0)$ theories, *Int. J. Mod. Phys. A* **28**, 1340006 (2013).
- [55] <https://www.antoinebourget.org/attachments/files/FissionDecay.nb>.
- [56] È. B. Vinberg and V. L. Popov, On a class of quasi-homogeneous affine varieties, *Math. USSR-Izvestiya* **6**, 743 (1972).
- [57] N. Nekrasov and V. Pestun, Seiberg-Witten geometry of four dimensional $N = 2$ quiver gauge theories, *SIGMA* **19**, 047 (2023).
- [58] A. Hanany and N. Mekareeya, Tri-vertices and $SU(2)$'s, *J. High Energy Phys.* **02** (2011) 069.
- [59] Z. Zhong (private communication).
- [60] A. Bourget, J. F. Grimminger, A. Hanany, M. Sperling, and Z. Zhong, Branes, quivers, and the affine Grassmannian, *Adv. Stud. Pure Math.* **88**, 331 (2023).
- [61] A. Hanany and E. Witten, Type IIB superstrings, BPS monopoles, and three-dimensional gauge dynamics, *Nucl. Phys.* **B492**, 152 (1997).
- [62] W. Crawley-Boevey, Geometry of the moment map for representations of quivers, *Compos. Math.* **126**, 257 (2001).
- [63] W. Crawley-Boevey, Normality of Marsden-Weinstein reductions for representations of quivers, [arXiv:math/0105247](https://arxiv.org/abs/math/0105247).
- [64] G. Bellamy and T. Schedler, Symplectic resolutions of quiver varieties, *Sel. Math.* **27**, 36 (2021).
- [65] J. Gu, Y. Jiang, and M. Sperling, Rational Q -systems, Higgsing and mirror symmetry, *SciPost Phys.* **14**, 034 (2023).
- [66] D. Gaiotto, $N = 2$ dualities, *J. High Energy Phys.* **08** (2012) 034.
- [67] A. Bourget, J. F. Grimminger, A. Hanany, R. Kalveks, and Z. Zhong, Higgs branches of U/SU quivers via brane locking, *J. High Energy Phys.* **08** (2022) 061.
- [68] N. Seiberg and E. Witten, Monopoles, duality and chiral symmetry breaking in $N = 2$ supersymmetric QCD, *Nucl. Phys.* **B431**, 484 (1994).
- [69] N. Seiberg and E. Witten, Electric-magnetic duality, monopole condensation, and confinement in $N = 2$ supersymmetric Yang-Mills theory, *Nucl. Phys.* **B426**, 19 (1994).
- [70] P. C. Argyres and M. R. Douglas, New phenomena in $SU(3)$ supersymmetric gauge theory, *Nucl. Phys.* **B448**, 93 (1995).
- [71] P. C. Argyres, M. R. Plesser, N. Seiberg, and E. Witten, New $N = 2$ superconformal field theories in four-dimensions, *Nucl. Phys.* **B461**, 71 (1996).
- [72] P. C. Argyres, M. R. Plesser, and N. Seiberg, The moduli space of vacua of $N = 2$ SUSY QCD and duality in $N = 1$ SUSY QCD, *Nucl. Phys.* **B471**, 159 (1996).
- [73] D. Gaiotto, G. W. Moore, and A. Neitzke, Wall-crossing, Hitchin Systems, and the WKB approximation, *Adv. Math.* **234**, 239 (2013).
- [74] P. C. Argyres and N. Seiberg, S-duality in $N = 2$ supersymmetric gauge theories, *J. High Energy Phys.* **12** (2007) 088.
- [75] F. Benini, Y. Tachikawa, and D. Xie, Mirrors of 3d Sicilian theories, *J. High Energy Phys.* **09** (2010) 063.
- [76] O. Chacaltana and J. Distler, Tinkertoys for Gaiotto duality, *J. High Energy Phys.* **11** (2010) 099.
- [77] D. Xie, General Argyres-Douglas theory, *J. High Energy Phys.* **01** (2013) 100.
- [78] S. Giacomelli, N. Mekareeya, and M. Sacchi, New aspects of Argyres-Douglas theories and their dimensional reduction, *J. High Energy Phys.* **03** (2021) 242.
- [79] D. Xie, 3d mirror for Argyres-Douglas theories, [arXiv:2107.05258](https://arxiv.org/abs/2107.05258).
- [80] G. Zafrir, Compactifications of 5d SCFTs with a twist, *J. High Energy Phys.* **01** (2017) 097.
- [81] P. C. Argyres and M. Martone, The rank 2 classification problem I: Scale invariant geometries, [arXiv:2209.09248](https://arxiv.org/abs/2209.09248).
- [82] S. Cremonesi, G. Ferlito, A. Hanany, and N. Mekareeya, Instanton operators and the Higgs branch at infinite coupling, *J. High Energy Phys.* **04** (2017) 042.
- [83] J. J. Heckman, D. R. Morrison, T. Rudelius, and C. Vafa, Geometry of 6D RG flows, *J. High Energy Phys.* **09** (2015) 052.
- [84] J. J. Heckman and T. Rudelius, Evidence for C-theorems in 6D SCFTs, *J. High Energy Phys.* **09** (2015) 218.
- [85] J. J. Heckman, T. Rudelius, and A. Tomasiello, 6D RG flows and nilpotent hierarchies, *J. High Energy Phys.* **07** (2016) 082.
- [86] N. Mekareeya, T. Rudelius, and A. Tomasiello, T-branes, anomalies and moduli spaces in 6D SCFTs, *J. High Energy Phys.* **10** (2017) 158.
- [87] F. Hassler, J. J. Heckman, T. B. Rochais, T. Rudelius, and H. Y. Zhang, T-branes, string junctions, and 6D SCFTs, *Phys. Rev. D* **101**, 086018 (2020).
- [88] F. Baume, M. J. Kang, and C. Lawrie, Two 6D origins of 4D SCFTs: Class S and 6D (1, 0) on a torus, *Phys. Rev. D* **106**, 086003 (2022).
- [89] N. Mekareeya, K. Ohmori, Y. Tachikawa, and G. Zafrir, E_8 instantons on type-A ALE spaces and supersymmetric field theories, *J. High Energy Phys.* **09** (2017) 144.
- [90] M. Del Zotto and G. Lockhart, Universal features of BPS strings in six-dimensional SCFTs, *J. High Energy Phys.* **08** (2018) 173.
- [91] C. Cordova, T. T. Dumitrescu, and K. Intriligator, Anomalies, renormalization group flows, and the a-theorem in six-dimensional (1, 0) theories, *J. High Energy Phys.* **10** (2016) 080.
- [92] M. Del Zotto, M. Liu, and P.-K. Oehlmann, Back to heterotic strings on ALE spaces. Part I. Instantons, 2-groups and T-duality, *J. High Energy Phys.* **01** (2023) 176.
- [93] A. Beauville, Symplectic singularities, *Inventiones Math.* **139**, 541 (2000).
- [94] M. Fluder and C. F. Uhlemann, Evidence for a 5d F-theorem, *J. High Energy Phys.* **02** (2021) 192.